J. Membrane Biol. 97, 137–159 (1987)

The Journal of
Membrane Biology
© Springer-Verlag New York Inc. 1987

Ion Permeation through Single Channels Activated by Acetylcholine in Denervated Toad Sartorius Skeletal Muscle Fibers: Effects of Alkali Cations

Nino Quartararo, Peter H. Barry, and Peter W. Gage*
School of Physiology and Pharmacology, University of New South Wales, Sydney, Australia

Summary. The gigaohm seal technique was used to study ion permeation through acetylcholine-activated channels in cell-attached patches of the extrajunctional membrane of chronically denervated, enzyme-treated cells from the sartorius muscle of the toad *Bufo marinus*. The most frequently occurring channel type (>95% of channel openings), provisionally classified as 'extrajunctional,' had a chord conductance of approximately 25 pS under normal conditions (−70 mV, 11°C, Normal Toad Ringer's). The less frequently observed channel type (<5% of channel openings), classified as a 'junctional' type, had a conductance of 35 pS under the same conditions, and a similar null potential. In many patches, a small percentage (usually <2%) of openings of the extrajunctional channel displayed a lower conductance state. The shape of the *I-V* curves obtained for the extrajunctional channel depended on the predominant extracellular cation. For Cs and K, the *I-V* curves were essentially linear over the voltage range +50 to −150 mV across the patch, suggesting that the potential independent component of the energy profile within the channel was symmetrical. For Li, the *I-V* curve was very nonlinear, displaying a significant sublinearity at hyperpolarized potentials. Both an electrodiffusion and a symmetrical uniform four-barrier, three-site rate-theory model provided reasonable fits to the data, whereas symmetrical two-barrier, single-site rate-theory models did not. For the alkali cations examined, the relative permeability sequence was $P_{Cs} > P_K > P_{Na} > P_{Li}$—a "proportional" selectivity sequence. This was different from the single channel conductance sequence which was found to be $\gamma_K > \gamma_{Cs} > \gamma_{Na} > \gamma_{Li}$ implying that ions do not move independently through the channel. The relative binding constant sequence for the channel sites was found to be a "polarizability" sequence, i.e., $K_{Li} > K_{Cs} > K_{Na} > K_K$. There was an inverse relationship between the relative binding constant and the relative mobility for the cations examined. Under conditions when the single-channel conductance was relatively high, the conductance at depolarized potentials was lower than that predicted by both electrodiffusion and rate theory models, suggesting that there was a rate-limiting access step for ions, from the intracellular compartment into the channel.

Key Words ions · ion permeation · ion selectivity · channels · single channels · ACh channels · alkali cations · gigaohm seal technique · patch clamp · skeletal muscle · electrodiffusion · rate theory

Introduction

Studies of the selectivity of ion permeation through ACh-activated channels, based on measurements of null potentials from which estimates of relative permeabilities have been obtained, have shown that these channels are (1) cation selective with no significant anion permeation and (2) that there is little apparent selectivity between cations (Takeuchi & Takeuchi, 1959; Van Helden et al., 1977; Maeno et al., 1977). Relative permeabilities of organic cations, measured from null potentials, have given a fairly detailed structural configuration of the minimum cross-sectional region of these channels (Dwyer et al., 1980). In earlier experiments, endplate currents were used to estimate this null potential (e.g. Takeuchi & Takeuchi, 1960). In later experiments analysis of current fluctuations (noise analysis, e.g. Anderson & Stevens, 1973) was employed to obtain an *indirect* measure of the *average single-channel conductance* of a population of endplate channels. This technique allowed channel conductance to be measured as a function of membrane potential. It has also been shown (Barry et al., 1979; Takeda et al., 1980; 1982*a*,*b*; Barry & Gage, 1984) that analysis of measured null potentials and the voltage dependence of conductance of these channels allows the underlying ion permeation parameters—equilibrium 'binding' constants for electronegative sites within the channels and the relative ionic mobility (electrodiffusion models) within the channels or transition rate constant (rate-theory models)—to be deduced. The results showed clearly that there was a significant underlying equilibrium selectivity of these sites within the channels.

* *Current Address:* Department of Physiology, The John Curtin School of Medical Research, The Australian National University, Canberra, A.C.T., 2601.

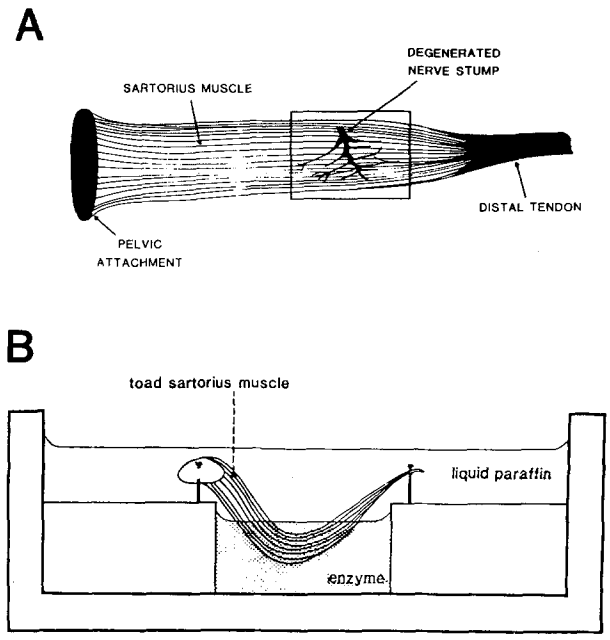

Fig. 1. (*A*) A schematic diagram of a chronically denervated sartorius muscle of the toad *Bufo marinus*. The area of the muscle enclosed by the rectangle shows the site where gross connective tissue was cleared using fine dissection just prior to the enzyme treatment. The area includes the site of the former end plate. All patches used for recording were from this area of the muscle. The most successful site within this area was usually at the edges of the muscle. The fibers at the edge of the muscle were easier to separate from one another and place on the fine glass supporting hook. They also appeared in many cases to have less tenacious connective tissue surrounding them but this may have been due to the better access for the enzymes to this region of the muscle. (*B*) The arrangement used to enzyme treat the sartorius muscle. The liquid paraffin was used to protect the tendons from enzymatic digestion. It also prevented dehydration of the portion of the muscle not in the enzyme solution. The enzyme solution was restricted to the well in the Sylgard (Dow-Corning) base of the Perspex® tissue bath. The enzyme solution could be introduced or removed from under the liquid paraffin using a Pasteur pipette. During enzyme treatment the muscle was incubated at a temperature of approximately 28°C. The same Perspex tissue bath was used for recording and enzyme treatment. This avoided the damage that may have occurred if the muscle was transferred after enzyme treatment to another bath for recording

The noise analysis technique has several drawbacks. It is indirect and depends on assumptions about individual channel events. Furthermore, only populations of channels can be studied and it is difficult to obtain an accurate measurement of single-channel conductance.

Previous studies in our laboratory (Van Helden et al., 1977; Barry et al., 1979; Gage & Van Helden, 1979; Gage & Hamill, 1980; Takeda et al., 1980; 1982*a*,*b*) had been carried out on the sartorius muscle of the toad *Bufo marinus*. The aim in the present study was to record directly the effects of permeant ions on end-plate channels using the patch-clamp technique on the same preparation.

Permeability ratios, as measured by the zero-current or null potential, have been the traditional criteria for measuring the selectivity of a channel. Originally, on the basis of permeability ratios, the end-plate channel was envisaged as a simple aqueous pore exerting little selectivity among the alkali cations. It has been shown that a variety of permeation models (Hille, 1975*b*; Barry & Gage, 1984) give rise to an expression for the null potential that is identical to the classical Goldman, Hodgkin, Katz (GHK) equation (Goldman, 1943; Hodgkin & Katz, 1949). It has also been shown for simple rate-theory (Hille, 1975*b*) and electrodiffusion models (Barry et al., 1979; Barry & Gage, 1984) that the permeability factor in the GHK equation is formally equivalent to the product of a transition rate constant (between wells or sites), or a mobility, and an equilibrium binding constant with respect to the aqueous solution. For simple rate-theory models it is obvious that the binding constant and mobility will tend to be inversely related. The deeper the well, the greater the binding constant, the higher the energy barrier between sites, and hence the lower the mobility. This has also been noted for electrodiffusion models (Barry et al., 1979) and would explain why the permeability ratio is a fairly insensitive measure of channel selectivity that may mask the equilibrium binding constant which is a much more sensitive measure of channel selectivity.

The aim of this study was therefore to measure the current-voltage relationship of an acetylcholine-activated channel present in the membrane of denervated adult muscle cells using the gigaohm seal technique, in the presence of various alkali cations. Rate-theory and electrodiffusion models were then fitted to the current-voltage curves obtained in order to extract equilibrium binding constants and mobilities for the various cations and derive more information about the process of permeation through these channels.

Materials and Methods

Preparation

All experiments were carried out on the denervated sartorius muscle of the toad *Bufo marinus*. The toads were denervated 4 to 6 weeks prior to the experiment. The area of the muscle from which patches were obtained is shown in Fig. 1*A*.

Solutions

Tetrodotoxin (TTX) at a concentration of 250 nmol liter^{-1} was used in all solutions to prevent muscle contractions. Monovalent

cations were substituted for Na by approximately equimolar replacement of NaCl with the chloride salt of the test cation. Table 1 gives the compositions of the alkali cation solutions tested. The bath solution had a volume of 3 to 4 ml and its temperature was maintained at 11°C during experiments.

Enzyme Treatment

After fine dissection to remove gross connective tissue surrounding the former end plate, the muscle was transferred to the tissue bath and pinned out so that approximately the middle third was suspended in the well in the Sylgard (Dow Corning) base of the bath (*see* Fig. 1*B*). The NTR in the tissue bath was removed using a Pasteur pipette and a small volume of enzyme solution introduced, just sufficient to cover the part of the muscle in the well. Liquid paraffin was then poured over the muscle so that it covered the tendons. The paraffin protected the tendons from enzymatic digestion and also prevented dehydration of the ends of the muscle. The tissue bath was then transferred to the experimental setup and placed in a temperature-controlled brass jacket. The temperature in the bath was maintained at approximately 28°C for the duration of the enzyme treatment. The enzyme solution was changed every 10 to 15 min with enzyme solution at approximately the same temperature. Care was always taken to minimize the mechanical disturbance to the muscle during exposure to enzyme solution and the changing of the enzyme solution was carried out using a Pasteur pipette to withdraw and introduce solution below the liquid paraffin.

The two enzymes used were collagenase (Type IA, Sigma Chemicals, St. Louis, Mo.) and protease (Type VII, Sigma Chemicals) at concentrations of 0.3% (300 mg/100 ml of NTR) in NTR and 0.04% (40 mg/100 ml of NTR), respectively. The exposure times were from 50 to 80 min in collagenase and 5 to 15 min in protease. After approximately 40 min of exposure to the collagenase and during exposure to the protease, the condition of the muscle was checked frequently. Enzyme treatment was stopped when the fibers at the edge of the muscle appeared clean and almost transparent and could be easily separated from each other by a gentle puff of solution from the Pasteur pipette. To stop enzyme treatment, NTR at approximately 28°C was added to raise the solution level until it covered the tendons. The paraffin was then separated from the surface. The muscle was repinned at approximately its resting length and the solution changed at least 20 times with NTR.

Patch-Clamp Methods

Patch-clamp methods were essentially the same as those of Hamill et al. (1981). Measurements were made with a current-to-voltage converter (List EPC-5). The electrodes were made from "soft" soda glass microhematocrit tubing (Clay-Adams, Parsippany, N.J., Type 1021, inner diam. 1.10 mm, outer diam. 1.50 mm). To offset the higher noise associated with soda glass (*see* for example, Corey & Stevens, 1983), the electrodes were coated with Sylgard (Dow Corning) to within about 300 μm of the tip and then fire-polished. A fine glass hook, made with a microforge, was used to support muscle fibers (Neher et al., 1978) as shown in Fig. 2.

The patch-clamp signal, after being appropriately amplified, was recorded using an FM analog tape recorder (Electrodata Associates, Sydney, Model 6504). The data were later played back for analysis by computer.

Table 1. Composition of alkali cation solutions[a] (mM) and calculated liquid junction potentials ($\mathscr{E}_L$) (mV)

Solution	NaCl	KCl	$CaCl_2$	CsCl	LiCl	($\mathscr{E}_L$)[b]
Na (NTR)	115	2.5	1.8	—	—	0.0
K	—	122.5	1.8	—	—	4.2
Cs	—	2.5	1.8	120	—	4.9
Li	—	2.5	1.8	—	120	−2.4

[a] All solutions contained 250 nM TTX and 3 mM sodium HEPES buffer.

[b] $\mathscr{E}_L$ was calculated using the Generalized Henderson Equation [Eqs. (7) and (8) in the text], in each case the potential being defined as that of the bath (NTR) with respect to the solution in the patch pipette.

To estimate current amplitude, at least ten but usually many more currents with "lifetimes" long enough to demonstrate an unequivocal steady state were recorded at each potential. The usual potential range was from −150 mV to +50 mV net across the patch. Currents were recorded at 20-mV steps in potential in this range. In many cases, currents were recorded over the full range of potentials from the same patch. Records used for the estimation of current-voltage curves were low-pass filtered at 1 kHz using the two-pole Bessel filter of the List patch-clamp controller, amplified appropriately and recorded on analog tape (bandwidth DC-2.5 kHz). Data were analyzed by computer. At potentials close to the null potential, it was necessary to further low-pass filter the record prior to digitization (usually at 200 or 400 Hz using a four-pole Bessel filter).

Intracellular Potential Recording

Standard intracellular recording techniques were used. In particular, the intracellular electrode was a 3-M KCl fiber-filled microelectrode with a Ag/AgCl junction and the reference ground electrode in the bath was a Ag/AgCl wire in NTR (gelled with 3% agar). At the end of recording, the intracellular electrode was withdrawn and checked to ascertain whether its tip and junction potentials had changed following penetration of the cell. Before each attempt at obtaining a seal, the solution in the bath was refreshed with solution at the same temperature and debris cleaned from the surface with a suction pump. All potential measurements were adjusted for junction potentials, as outlined in the later section on junction potential corrections.

Principles Underlying Experimental Techniques

When recording in the cell-attached mode, the return pathway for current involves the resistance of the cell membrane excluding the portion patch clamped. When a channel opens, current flows across this resistance thereby altering the cell resting potential and causing a change in the voltage across the membrane patch V_p.

A simplified circuit diagram, of the cell-attached recording configuration, similar to that of Fenwick et al. (1982) is shown in Fig. 3. The circuit is an oversimplification since the muscle cell has been modelled as a parallel *R/C* circuit rather than the more appropriate linear cable model. The response of the circuit to a

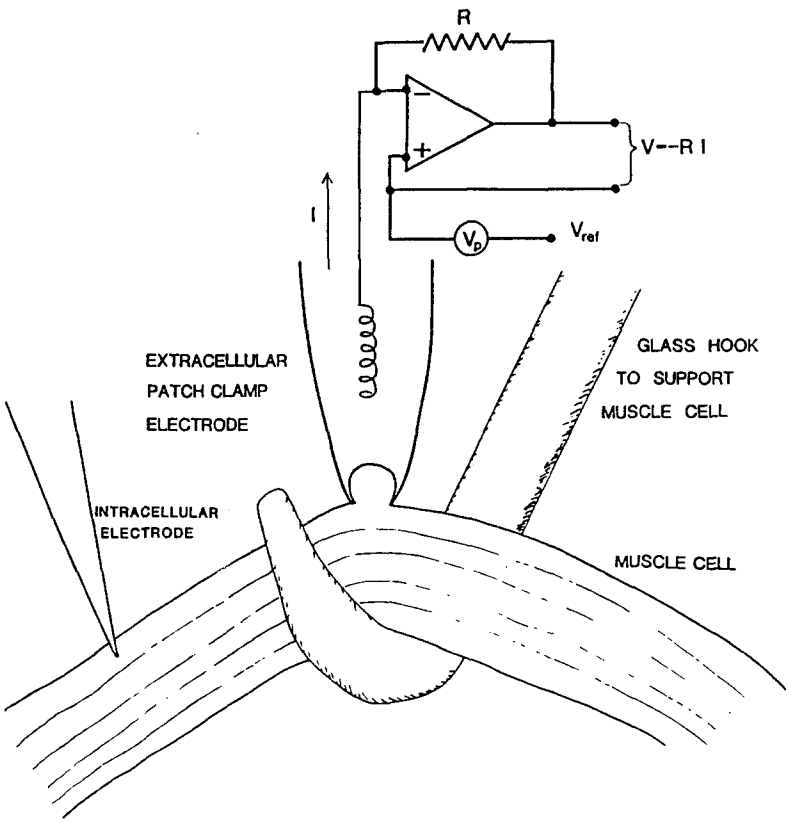

Fig. 2. A simplified schematic diagram of the recording configuration. After enzyme treatment the fine glass hook was used to separate out and support a single muscle cell. An intracellular electrode was then inserted into the muscle cell to monitor the resting membrane potential. This was used as explained in the text to determine the potential across the patch of membrane. This potential could be changed using the d-c voltage source V_p. Usually when a gigaohm seal is formed a patch of membrane is sucked into the tip of the patch-clamp electrode (Sakmann & Neher, 1983). This approximately omega-shaped patch of membrane is shown in the tip of the patch-clamp electrode

step change in the conductance of the patch when a channel opens can readily be shown to be given by:

$$V_p(t) = V\{G - (G - G_m/(G_m + G_p)) \exp(-t/\tau)\} \quad (1)$$

where

$$G = G_m/(G_m + G_p + \gamma_{CH}) \quad (2)$$

$$\tau = C_m/(G_m + G_p + \gamma_{CH}) \quad (3)$$

$$V = V_m - V_{\text{pol}}. \quad (4)$$

G_p is the conductance of the patch, G_m is the input conductance of the muscle cell, C_m is the input capacitance of the muscle cell, γ_{CH} is the conductance of the channel, V_m is the resting membrane potential of the cell, V_{pol} is the potential applied to the electrode. At $t = 0$:

$$V_p(0) = VG_m/(G_m + G_p)). \quad (5)$$

This is a simple voltage divider formed by G_p in series with G_m. At $t = \infty$:

$$V_p(\infty) = VG_m/(G_m + G_p + \gamma_{CH}). \quad (6)$$

This is also a simple voltage divider but this time the parallel combination of G_p and γ_{CH} is in series with G_m. Assuming a specific patch resistance of $10^3\ \Omega \cdot \text{cm}^2$ (Fenwick et al., 1982) and an upper limit of 30 μm^2 for the area of the patch (Hamill et al., 1981; Sakmann & Neher, 1983; Rae & Levis, 1984) gives $G_p \approx$ 300 pS ($R_p \approx 3$ GΩ). Normally the apparent seal resistance was greater than 20 GΩ indicating one or both of the above assumptions overcompensated. Assuming a channel conductance (γ_{CH}) of 25 pS and an input conductance (G_m) of 2×10^{-6} S (Dulhunty & Gage, 1973), it is found from Eqs. (5) and (6) that $V_p(0) \approx V_p(\infty) \approx V$. In other words, the opening of the channel has a negligible effect on the potential across the patch because of the relatively low input resistance of the cell. Similarly, it may be readily shown that V_{pol} does not significantly affect V_p.

It was possible that large portions of membrane were aspirated into the tip of the electrode when a gigaohm seal formed (Hamill et al., 1981; Sakmann & Neher, 1983; Rae & Levis, 1984). Under these circumstances, a pocket of cytoplasm could form in the tip of the electrode and the constriction of cytoplasm would then add a resistance in series with the cell input resistance. The resistance would not be expected to be much greater than the electrode resistance (≈8 MΩ) and so as explained earlier, should introduce a negligible error to the potential across the membrane patch. Appreciable change in the ionic composition of the pocket of cytoplasm did not seem to occur. On a number of occasions, the amplitudes of the currents were checked after a relatively long recording time (≈15 min) and found to be the same as at the commencement of recording. Both Maruyama and Petersen (1982) and Siegelbaum et al. (1982) (*see also* Camardo & Siegelbaum, 1983) have shown that the local bath application of active compounds can lead in a short time (20 to 40 sec, Maruyama & Petersen, 1982) to the activation of channels in a cell-attached patch. This indicates that there is a free exchange of materials between the contents of the pocket and the general cytoplasm.

Junction Potential Corrections

In the patch-clamp situation corrections due to (1) the normal junction potential component arising from the measurement of the membrane potential and (2) the junction potential component

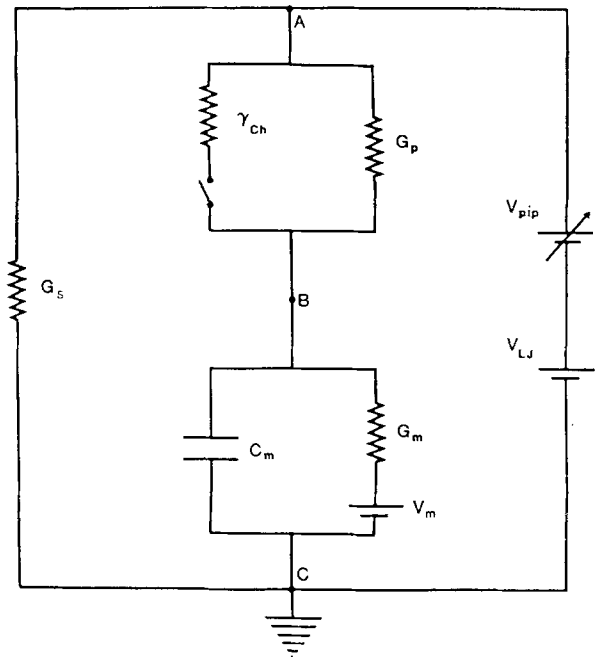

Fig. 3. Simplified equivalent circuit of the cell-attached patch-recording configuration: γ_{Ch} is the single-channel conductance, G_p is the conductance of the membrane patch, G_s is the conductance of the seal between the tip of the patch-clamp electrode and the cell membrane, G_m is the input conductance of the muscle cell, C_m is the input capacitance, V_m is the resting membrane potential of the muscle cell corrected for the liquid junction potential of the intracellular electrode, V_{pip} is the potential applied to the patch-clamp electrode and V_{LJ} is the liquid junction potential of the patch-clamp electrode. The reference points denote: A, the patch-clamp electrode solution, B, the cell interior and C, the bath solution. Note that the capacitance of the patch is negligible compared to C_m and so has been neglected

were calculated using the Generalized Henderson Liquid Junction Potential Equation. For N monovalent ions the potential $\mathscr{E} = (\mathscr{E}'' - \mathscr{E}')$ of the solution $''$ with respect to solution $'$ is given by

$$\mathscr{E} = \mathscr{E}'' - \mathscr{E}' = (RT/F)S_F \ln\left[\sum_{i=1}^{N} a_i' u_i \Big/ \sum_{i=1}^{N} a_i'' u_i\right] \tag{7}$$

where

$$S_F = \sum_{i=1}^{N} [(u_i/z_i)(a_i'' - a_i')] \Big/ \sum_{i=1}^{N} [u_i(a_i'' - a_i')] \tag{8}$$

where u, a and z represent the mobility, activity and valency (including sign) of each ion species. The equation (*cf.* MacInnes, 1961) has been modified (Barry & Diamond, 1970) to include activities rather than concentrations on the assumption that the ions obey the Guggenheim condition [i.e. that the individual activity coefficients of each ion are equal at every point in the solution, so that $\gamma_1(x) = \gamma_2(x) = \gamma_3(x) = \ldots = \gamma(x)$].

The first component, due to the normal difference in junction potentials between the intracellular and extracellular electrodes, was calculated from Eq. (9) below (*see* Fig. 4*A*). For example, for a typical NaCl Ringer's solution and high K^+ and low Cl^- intracellular composition and 3-M KCl electrodes, the

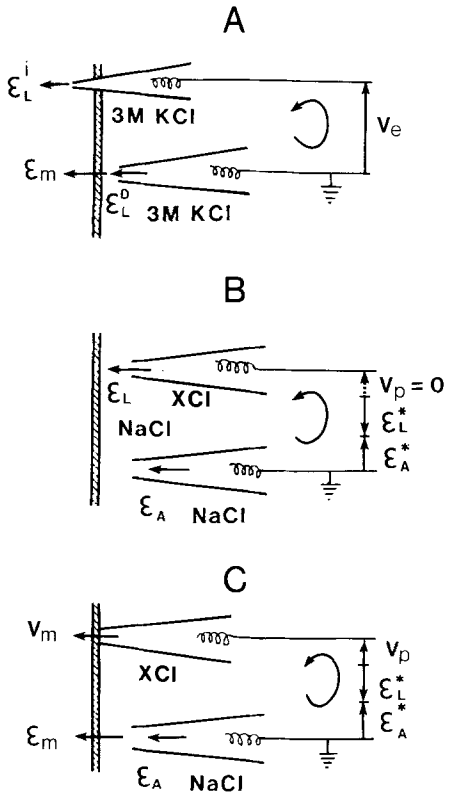

Fig. 4. A schematic diagram illustrating the measurement of transmembrane patch potentials using the patch-clamp technique for intact membrane patches and the application of junction potential corrections to such measurements. These corrections involve the normal junction potentials arising from the intracellular measurement of membrane potential (*A*) and the special correction that arises by virtue of the zeroing of the patch-clamp amplifier for an intact patch when the solution in the patch pipette differs from that in the solution bathing the cell (*B* and *C*). (*A*) The measurement of the membrane potential $\mathscr{E}_m$ with normal intracellular or extracellular 3-M KCl microelectrodes. Normally either the two Ag/AgCl electrodes would be balanced or at least backed off before the intracellular electrode was inserted into the cell. Applying Kirchoff's law in the anticlockwise direction as shown $V_e + \mathscr{E}_L^i - \mathscr{E}_m - \mathscr{E}_L^o = 0$, where V_e is the experimentally measured potential and $\mathscr{E}_L^i$ and $\mathscr{E}_L^o$ represent the two microelectrode junction potentials as shown. Thus $\mathscr{E}_m = V_e - (\mathscr{E}_L^o - \mathscr{E}_L^i)$ as in Eq. (9) in the text. (*B*) The zeroing of the patch-clamp pipette before a seal is established. For an NaCl bathing solution around the cell a reference electrode filled with NaCl should preferably be used. The patch pipette has a test solution (e.g., *X*Cl for a cation *X*) in it. There are two sources of inbalanced potential that need to be backed off by the patch-clamp amplifier. There will in general be a difference $\mathscr{E}_A$ between the two Ag/AgCl electrodes with slightly different Cl activity in both electrodes and pipette. There would also be a junction potential $\mathscr{E}_L$ between the NaCl and *X*Cl solutions. Both of these would be backed off in the amplifier by two voltage components $\mathscr{E}_A^*$ and $\mathscr{E}_L^*$ as indicated. The applied potential $V_P = 0$ and hence applying Kirchoff's law in the direction shown $\mathscr{E}_L - \mathscr{E}_A + \mathscr{E}_A^* - \mathscr{E}_L^* = 0$, which will be satisfied provided that $\mathscr{E}_L^* = \mathscr{E}_L$ and $\mathscr{E}_A^* = \mathscr{E}_A$. (*C*) The patch-clamp pipette sealed against the membrane. In this situation, the liquid junction potential correction $\mathscr{E}_L$ would have been eliminated, but the backed-off component would still be present. If a voltage V_P were then applied by the patch-clamp amplifier, again from Kirchoff's law $V_P + V_m - \mathscr{E}_m - \mathscr{E}_A + \mathscr{E}_A^* - \mathscr{E}_L^* = 0$ and so $V_m = (\mathscr{E}_m - V_P) + \mathscr{E}_L$ as in Eq. (11) in the text

corrected membrane potential ($\mathscr{E}_m$) is related to the measured membrane potential (V_e) by

$$\mathscr{E}_m = V_e - (\mathscr{E}_L^o - \mathscr{E}_L^i) \tag{9}$$

or

$$\mathscr{E}_m \approx V_e - 2.0 \tag{10}$$

where $\mathscr{E}_m$ and V_e are in mV and $\mathscr{E}_L^o$ and $\mathscr{E}_L^i$ refer to the liquid junction potentials at the external and internal microelectrodes, respectively, being defined as solution with respect to microelectrode.

The second junction potential component, arising by virtue of the necessary zeroing of the patch-clamp amplifier, whenever the solution in the patch-clamp pipette differs from that in the bathing solution was calculated as indicated in Fig. 4. The true potential V_m across the patch was given by

$$V_m = (\mathscr{E}_m - V_p) + \mathscr{E}_L \tag{11}$$

where V_p is the additional potential applied by the patch-clamp amplifier and $\mathscr{E}_L$ is defined as the potential of the external bathing solution with respect to the patch pipette. The same equations apply for the excised patch, together with the condition that $\mathscr{E}_m = 0$.

The correction applied for the liquid junction potential of the patch-clamp electrode was checked experimentally for both Li^+ and Cs^+ and found to agree with values calculated from the Planck or Generalized Henderson equations. Since the tip diameter of the patch-clamp electrode is approximately 1 μm, the electrical contact between the filling solution and that of the bath should form a simple diffusion or liquid junction (Gagne & Plamondon, 1983). Therefore the potential should be consistent for different electrodes with the same filling solution. To circumvent the application of the liquid junction potential correction, experiments were attempted using Cs^+ Ringer's solution both in the bath and in the patch-clamp electrode. This experiment was tried on five different preparations but was unsuccessful because the Cs^+ Ringer's bath solution caused significant depolarization of the cells (membrane potentials of -50 to -60 mV). Although gigaohm seals were formed, the seals were more unstable than those obtained with NTR bath solution.

The liquid junction potential correction applied to the potential recorded by the intracellular electrode depended on assumptions concerning the concentrations of intracellular ions and their mobilities. This was another possible source of error. Errors due to tip potentials were minimized by using low resistance intracellular electrodes (Purves, 1981).

Analysis of Data and Theoretical Model Fitting

The null potential was estimated by interpolation of the current-voltage curve. Firstly, a simple linear graphical method was used. This involved plotting the two points on either side of the null potential on an expanded voltage axis and drawing a line of best fit by eye through the points. The null potential was given by the intersection of this line with the voltage axis. Secondly, a curve was fitted by cubic regression to the 4 or 5 points in the vicinity of the null potential. The roots of this polynomial were determined and the appropriate root taken as another estimate of the null potential. It was this latter estimate that was used to calculate the experimental single-channel chord conductance $\gamma(V)$ using:

$$\gamma(V) = I(V)/(V - \mathscr{E}_o) \tag{12}$$

where $I(V)$ is the single-channel current at voltage V and $\mathscr{E}_o$ is the null potential. The standard error of the chord conductance was calculated using the formula for a general product (*see*, for example, Barford, 1967).

The current-voltage curves were used to test three models, an electrodiffusion model and two rate-theory models. An introduction to the models is given in the next section. The electrodiffusion model has been described by Barry et al. (1979), and used in that study to fit the data of Gage and Van Helden (1979). The first rate-theory model tested in the present study was symmetrical, with two uniform barriers and one site and was based on that of Lewis and Stevens (1979). The second rate-theory model tested was symmetrical, with four uniform barriers and three sites and was based on that of Hille (1975*a*).

The electrodiffusion model, after scaling, was fitted using a robust lattice searching with two adjustable or free parameters, the relative equilibrium binding constant K_X/K_K, and the relative permeability P_X/P_K. The scaling constant was determined using the current-voltage point which had the lowest relative standard error for the current. It was then maintained constant at this value for the rest of the fitting procedure. The objective function to be minimized was the weighted sum of the squared residuals, the weights being the inverses of the standard errors squared. As the program converged to a minimum, the contours of the sum of squared residuals surface were displayed. This confirmed by direct inspection that the point was a minimum and not a saddle point or some other relatively stationary portion of the surface.

The program FUNFIT supplied by the Computer Services Unit of the University of New South Wales was used to fit the rate-theory models to the current-voltage curves. The program was run on a VAX 11/780 computer (D.E.C.). Four free parameters were used to fit the rate-theory models to the sodium *I-V* data. The current carried by calcium was considered to be relatively small and was neglected (*see* Results section for details). Current was assumed to be carried by sodium and potassium only and the four free parameters were the barrier heights and well depths for sodium and potassium. For the lithium and caesium figures and the data

included in this paper, the current-voltage curves were fitted using four free parameters. In this case, the barrier height and well depth for sodium were set at the values found to give the best fit to the sodium *I-V* data and the four free parameters were the barrier heights and well depths for potassium and caesium or lithium. In addition, some two-parameter fits were also done, in which the barrier heights and well depths for sodium and potassium were assumed to be those found to give a best fit to the sodium *I-V* data and the two free parameters were the barrier height and well depth for lithium or caesium. The fits were not quite as good for Li as in the four-parameter case. There were also some differences in the derived parameters (e.g., for the two-parameter case P_{Li}/P_K, K_{Li}/K_K, u_{Li}/u_K = 0.53, 2.4 and 0.22 compared to the four-parameter values of 0.59, 3.6 and 0.17, respectively). In contrast, very similar results were obtained for Cs in both cases. However, in the light of the slightly poorer fitting, only the four-parameter fitted values have been included in the following sections.

Theoretical Models Tested

Before giving the results of the model fitting, a brief description of the models and the parameters used to fit the data will be given. It should be stressed that only the major conductive element or channel 'interior' was modelled and no attempt was made to incorporate structures such as antechambers (*see*, for example, Horn & Stevens, 1980).

The electrodiffusion model has been fully described by Barry et al. (1979) and a summarized account of the model is given by Barry and Gage (1984). The model assumes that the channel is long relative to the Debye length within the channel so that electroneutrality applies within the channel. Cations are assumed to compete for negative sites on neutral groups lining the channel. For example, cations could compete for the negative ends of dipoles lining the channel. The electroneutrality condition then requires that the charge of the cations is balanced by allowing anions to enter the channel. An assumption then has to be made that the overall mobility of anions is negligible (i.e., that there is at least one high resistance barrier to anions) so that anions make no significant contribution to the total ionic current. It should be pointed out that, due to the competition between cations for the negative sites, independence is violated. That is, the behavior of an ion is modified by the presence of similar or different ions. In contrast, the Independence Principle is implicit in the derivation of the traditional electrodiffusion equation, the Goldman, Hodgkin, Katz (GHK) equation. Another variation of the electrodiffusion model assumes that the channel sites have a net negative charge. Electroneutrality then requires that the negative charge of the sites be balanced by the mobile cations. As in the Neutral Site Model independence is violated. It should be stressed that the voltage-dependent part of the current expression for both models is identical but they differ in the voltage-independent factor and can be distinguished by examining the effects of changing the concentration of the extracellular cations on the channel conductance. The Charged Site Model predicts the conductance would be independent of concentration whereas the Neutral Site Model predicts the conductance would change with the external cation concentration. It has been well established that the conductance does vary with the external cation concentration (*see*, for example, Horn & Patlak, 1980; Takeda et al., 1982*a*). Hence in this study only the Neutral Site Model was tested. For the Neutral Site Model in the absence of significant anion permeation, the current I is given by:

$$I = B[(\xi u'' - u')/(\xi C'' - C')](\mathscr{E} - \mathscr{E}^*) \tag{13}$$

where

$$\xi = \exp(F\mathscr{E}/RT) \tag{14}$$

$$\mathscr{E}^* = (RT/F)\ln(C'/C'') \tag{15}$$

$$C' = a_1' + K_{21}a_2' + K_{41}a_4' \tag{16}$$

$$C'' = a_1'' + K_{21}a_2'' + K_{41}a_4'' \tag{17}$$

$$u' = u_1a_1' + u_2K_{21}a_2' + u_4K_{41}a_4' \tag{18}$$

$$u'' = u_1a_1'' + u_2K_{21}a_2'' + u_4K_{41}a_4'' \tag{19}$$

$$B = (F^2/d)(K_3/\gamma)A_F[(a_3'/\theta') - (a_3''/\theta'')]/\ln(a_3''\theta'/a_3'\theta'') \tag{20}$$

$$\theta' = [K_3a_3'/(a_1' + K_{21}a_2' + K_{41}a_4')]^{1/2} \tag{21}$$

$$\theta'' = [K_3a_3''/(a_1'' + K_{21}a_2'' + K_{41}a_4'')]^{1/2} \tag{22}$$

and where $\mathscr{E}$ is the membrane potential (inside with respect to outside), R, T and F have their usual significance, subscripts 1, 2 and 4 refer to cations and 3 to the anion; superscripts $'$ and $''$ refer to the outside and inside solutions, respectively; a represents the activity of the ion; u_i and K_{ij} denote the intra-channel mobility and equilibrium constant (K_{ij} representing the relative partition coefficients K_i/K_j) of ion i, respectively, relative to ion j; γ the activity coefficient, which is considered to be the same for each of the ions; and A_F is the effective cross-sectional area of the channel. It should be noted that the above expression for the current is of a very different form from that of the GHK current expression but that the equation for the null poten-

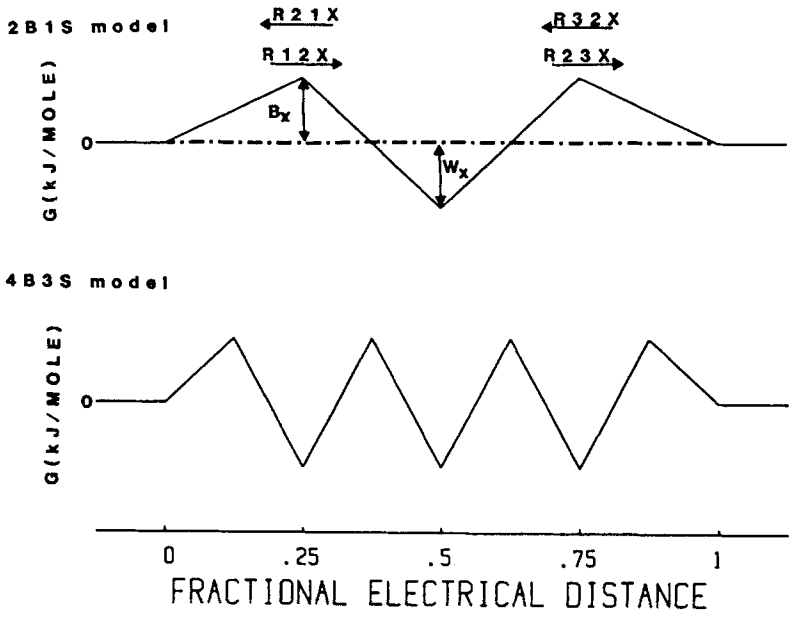

Fig. 5. Schematic diagram of two classes of rate-theory models used to fit experimental current-voltage curves. The top panel (2B1S model) shows the two-barrier, one-site model. The energy profile shown is the voltage-independent part of the Gibb's Free Energy (G). The aqueous solution at either end of the channel is taken as the zero reference level. B_x and W_x are the barrier height and well depth, respectively, for ion X. R12X, R21X, R32X, and R23X are rate constants for the passage of ions over the barriers in the energy profile. Their values are given by rate theory (*see text* for details). The bottom panel (4B3S model) shows a schematic diagram of the four-barrier, three-site model

tial is of the same form as the GHK equation (Barry et al., 1979).

It should be mentioned that the long Neutral Site Channel and long Charged Site Channel models differ only in their conductance-concentration predictions because of the applicability of the electroneutrality condition within them. It is therefore to be expected that if this condition were to be relaxed, as would be expected for a short Channel, then the resulting predictions of the short Charged Site Channel would become very similar to those of the long Neutral Site Channel, with the ionic concentration within the channel able to increase with its value within the external bathing solution.

Two rate-theory models were also tested in this study. The first was based on the model of Lewis and Stevens (1979). This was a symmetrical model and contained one site (i.e., energy minimum or well) and two uniform barriers (2B1S model). The model is shown schematically in Fig. 5*A*. The parameter d is the fractional electrical distance across the membrane. Initially the site was located at $d = 0.5$ and the barriers at $d = 0.25$ and $d = 0.75$. Both surface charge effects and the component of the current carried by calcium ions were neglected since their effects on the total current under experimental conditions was small. For instance, using approximate barrier heights and well depths given by Lewis and Stevens (1979) for calcium, and given an extracellular calcium concentration of 1.8 mM, the flux of calcium at −150 mV comprises only approximately 0.1% of the total current. Important assumptions of the model are that only one ion at most can be in the channel at any time and that an ion can only enter the channel if it is empty. The rate constants for passage over the barriers are given by conventional Eyring rate-theory (Eyring, 1935; Glasstone et al., 1941; Woodbury, 1971). Voltage dependence of the rate constants is incorporated by adding an electrical term to the Gibbs Free Energy of Activation of the process. Hence the rate constants depicted in Fig. 5 are given by:

$$R21X = \nu_1 \exp[(W_x - B_x + 0.25(Z_xFV))/RT] \quad (23)$$

$$R23X = \nu_1 \exp[(W_x - B_x - 0.25(Z_xFV))/RT] \quad (24)$$

$$R12X = [X]_o\nu_2 \exp[(-B_x - 0.25(Z_xFV))/RT] \quad (25)$$

$$R32X = [X]_i\nu_2 \exp[(-B_x + 0.25(Z_xFV))/RT] \quad (26)$$

where ν_1, ν_2 are frequency factors given values 10^{13} sec^{-1} and 10^{11} $molar^{-1}$ sec^{-1}, respectively (Lewis & Stevens, 1979); $[X]_o$ and $[X]_i$ are the extracellular and intracellular concentrations of ion X, respectively; R, T and F have their usual thermodynamic meaning; V is the net potential across the membrane patch with respect to the electrode solution; Z_x is the valence of ion X; B_x is the barrier height (kJ/mole) for ion X taken relative to the aqueous solution; and W_x is the well depth (kJ/mole) for ion X taken relative to the aqueous solution. The derivation of, and the expression for, the current as a function of the potential is given by Lewis and Stevens (1979). Note that because of the symmetry of the channel the constant peak offset condition of Hille (1975*b*) applies and the permeability as defined in the Generalized Null Potential Equation (Barry & Gage, 1984; *see also* Hille, 1975*b*) is given by the barrier height only and is not influenced by the well

depth. This Generalized Null Potential Equation is essentially model-independent and applies to a large number of different models in the absence of any significant anion permeation. The zero current null potential $\mathscr{E}_o$ is given by

$$\mathscr{E}_o = \mathscr{E}'' - \mathscr{E}' = \frac{RT}{F} \ln \left\{ \frac{P_1 a_1' + P_2 a_2' + P_4 a_4'}{P_1 a_1'' + P_2 a_2'' + P_4 a_4''} \right\} \quad (27)$$

where ' and " refer to the two solutions on sides ' and ", respectively, a refers to the activity of cations 1, 2 and 4 (3 being reserved for anions). The relative permeabilities are related to the underlying equilibrium constants K and ionic mobilities u by

$$P_1/P_2 = (u_1/u_2)(K_1/K_2). \quad (28)$$

The second rate-theory model tested in this study, based on a model of Hille (1975*a*) was a 4-barrier, 3-site model (4B3S model) simplified for symmetrical and uniform barriers. As in the case of the previous model, only one ion at most is allowed in the channel at any time and an ion can only enter the channel if it is unoccupied. A schematic diagram of the model is given in Fig. 5. Expressions for the rate constants in terms of the barrier heights, well depths and membrane potential are derived using precisely the same principles as for the previous model. Because of the symmetry, only four rate constants have to be calculated. The four expressions for the rate constants are similar to those given previously for the 2B1S model but with two changes. ν_1 and ν_2, the frequency factors, were equal numerically and given by kT/h where k is Boltzmann's constant, h is Planck's constant and T is the absolute temperature in degrees Kelvin. At 5°C, ν_1 and ν_2 were approximately 5.8×10^{12}. The factor 0.25 in the expressions for the rate constants of the 2B1S model was replaced by the factor 0.125, so the barrier energy was only half as voltage-dependent for the 4B3S model. The expression for the current as a function of the membrane potential is given by Hille (1975*a*). Because of the somewhat arbitrary choice of the value of the frequency factor, the absolute barrier heights and well depths fitted were used only to calculate permeation and selectivity parameters relative to those for potassium, the reference ion. The parameters were related to the barrier height and well depth by the following relations:

the relative binding constant, K_X/K_K, of ion X

$$K_X/K_K = \exp[-(W_X - W_K)/RT] \quad (29)$$

where W_X and W_K are the well depths of ion X and potassium, respectively, and R and T have their usual significance;

the relative permeability, P_X/P_K, of ion X

$$P_X/P_K = \exp[-(B_X - B_K)/RT] \quad (30)$$

where B_X and B_K are the barrier heights of ion X and potassium, respectively;

the relative mobility, u_X/u_K, of ion X

$$u_X/u_K = (P_X/P_K)/(K_X/K_K). \quad (31)$$

Only symmetrical rate-theory models were considered for several reasons (*see also* discussion in sections: *Results of Model Fitting* and *Effects of Alkali Cations*). Firstly, the current-voltage curves recorded with potassium and caesium as the predominant extracellular cations were practically linear (*see* Fig. 9). In the case of potassium, the membrane was bathed by approximately symmetrical solutions. Also, in view of the chemical similarities between caesium and potassium (Hille, 1975*b*; Barry & Gage, 1984) both ions would be expected to behave similarly with respect to permeation. Hence under these experimental conditions (potassium and caesium as external cations) any significant energy barrier asymmetry in the channel should have been revealed by the finding of a significantly non-symmetrical current-voltage curve. Secondly, recent studies using excised patches from cultured cells have found that the current-voltage curve for ACh channels bathed in symmetrical alkali cation solutions is linear (Horn & Patlak, 1980; Redmann et al., 1982; Dwyer & Farley, 1984; Dwyer, 1986; Sanchez et al., 1986).

Results

Channel Types and Subconductance States

Three types of ACh-sensitive channels with different conductances were observed as illustrated in Fig. 6*A* and 6*B*. At a potential of −70 mV and at 11°C, one had a conductance of about 35 pS, another 25 pS and a third, normally very uncommon, type had a conductance of approximately 18 to 20 pS. The first two were classified as 'junctional' and 'extrajunctional,' respectively. The 'junctional' channels accounted for less than 5% of the channel openings, whereas the 'extrajunctional' channels accounted for at least 95% of channel openings. Current-voltage curves for junctional (circles) and extrajunctional (squares) channels in the same patches exposed to the Na solutions are shown in Fig. 7. The extrapolated lines indicate (1) that both

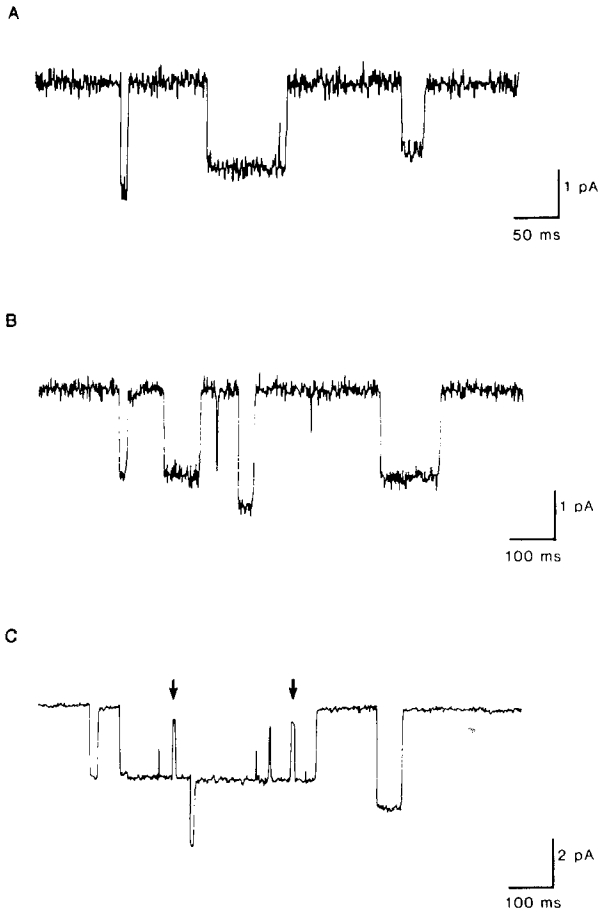

Fig. 6. Some examples of the different apparent types of ACh-activated channels observed. All records were obtained using NTR (*see* Table 1). Temperature 11°C. *A*, recorded at a net patch potential of −70 mV, coincidently shows the most commonly occurring "25 pS," extrajunctional channel together with the less frequently occurring junctional channel before its occurrence and the very infrequently lower conductance channel afterwards (low-pass filtered at 1 kHz). *B*, recorded at a net patch potential of −70 mV, shows the two most commonly occurring channel types (low-pass filtered at 1 kHz). *C*, recorded at a net patch potential of −130 mV, shows the two most frequently occurring channel types, with the extrajunctional channel exhibiting low conductance states (arrows; low-pass filtered at 800 Hz)

channels had approximately the same null potential and (2) that the ratio of the conductances of both channels was independent of voltage and equal to 1.4 (Fig. 7*B*). In all the later sections of this paper, only the measurements from the much more numerous extrajunctional channels will be considered. Although they were very infrequent, in less than 2% of the extrajunctional channel openings, a lower subconductance state was also observed (Fig. 6*C*, *cf.* Hamill & Sakmann, 1981).

Current-Voltage Curves in Different Cation Solutions

At +50 mV (net across the patch) the amplitudes of the currents recorded in different cation solutions were approximately the same, whereas at −150 mV the amplitudes differed markedly. This is illustrated in Fig. 8, which shows larger currents in Cs than Li solution at −150 and at −70 mV, but not at +50 mV.

The current-voltage curves recorded in four different cation solutions (Na, Li, Cs, K) are shown in Fig. 9. In a number of patches in each solution the currents were recorded over the full potential range. Most points on the curves represent results from at least six different preparations. It can be seen that the degree of nonlinearity of the curves depends on the extracellular cation. The curves for Cs and K are essentially linear while that for Li shows a marked curvature. In the case of Na, the curvature is slight but definite. Both the Na and Li curves show an outward rectification; that is, at hyperpolarized potentials, there is a drop in the conductance which is more pronounced for Li.

The Null Potential in Different Cation Solutions

The *I-V* curves in Fig. 9 also show that the null potential varies with the extracellular cation. The null potentials in the various cation solutions were estimated by linear and cubic interpolation using the appropriate points on the *I-V* curve. The results of this are given in Table 2. The estimates obtained from the two methods agree reasonably well except in the case of Li. This is understandable since the lithium *I-V* curve displayed by far the greatest nonlinearity. Both methods gave the same sequence of null potentials: Li < Na < K < Cs. This is the same sequence found by Van Helden et al. (1977) and Gage and Van Helden (1979) using noise analysis on junctional channels from innervated toad sartorius muscle.

The permeability ratios corresponding to the null potentials were found by numerically solving the Generalized Null Potential Equation (Eqs. 12 & 13; *see also* Barry & Gage, 1984) using the Newton-Raphson method. The results are given in Table 2. The permeability sequence found was Cs > K > Na > Li. This is the same sequence as has been reported previously for junctional amphibian endplate channels obtained using macroscopic techniques (*see*, for example, Van Helden et al., 1977; Gage & Van Helden, 1979; Adams et al., 1980) and

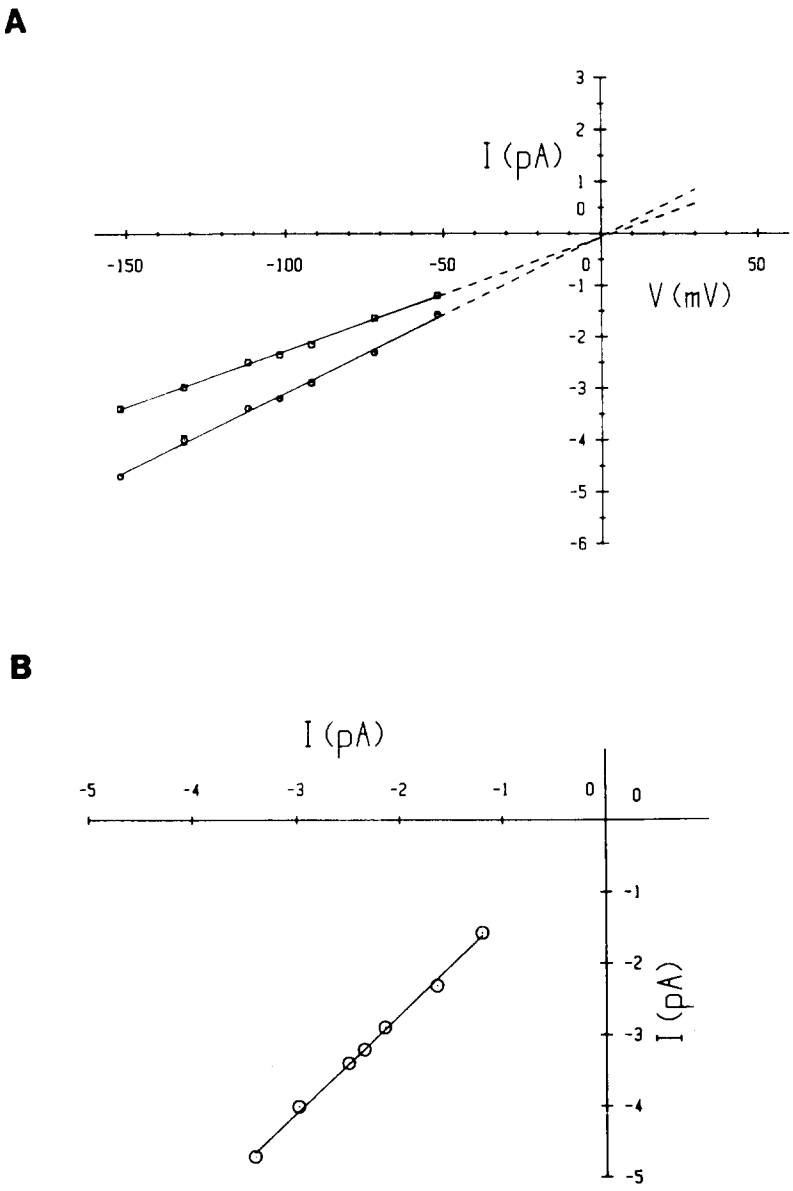

Fig. 7. (*A*) An experimental current-voltage curve for "extrajunctional" (squares) and "junctional" (circles) channels. Solid lines represent least-squares regression lines fitted to each set of points. The slopes of these lines gave slope conductances of 22 and 30 pS for "extrajunctional" and "junctional" channel types, respectively. The dashed lines were used to estimate the null potential by extrapolation. The null potential was similar for both channel types. Data were obtained from the pooled results of eight patches recorded using the Na test solution (NTR) in the patch-clamp electrode. The electrode solution also contained ACh (100 to 300 nM). The error bars represent ±1 SEM and are not shown if smaller than the symbol size. Temperature 11°C. (*B*) The same data as *A*, but replotted as the "junctional" channel current versus the "extrajunctional" channel current at each potential. The line was fitted using least-squares regression. The slope of this line gave a value for the ratio γ(junctional)/γ(extrajunctional) ≈1.4

is the same as the aqueous mobility sequence for the ions (Robinson & Stokes, 1965).

Conductance-Voltage Curve in Different Cation Solutions

Since the current at a particular potential is given by the product of the chord conductance and the driving force (the difference between the potential and the null potential) it is instructive to determine the chord conductance-voltage curve to separate out these two factors. The equation used to calculate the chord conductance has been given in Materials and Methods. The estimate of the null potential obtained by cubic interpolation was used to calculate the chord conductance for each cation solution.

The chord conductance-voltage curves for each cation solution are shown in Fig. 10. At −150 mV the major part of the current is carried by the extracellular cation. Examination of the conductance at −150 mV for each of the cation solutions reveals that conductance depends on the extracellular cation. It would appear then, that the extracellular cation not only sets the null potential but also the conductance of the channel, particularly at negative potentials. The conductance sequence is K > Cs > Na > Li and is different from the permeability sequence mentioned above. This indicates that independence is violated (Hille, 1975*b*) since, if in-

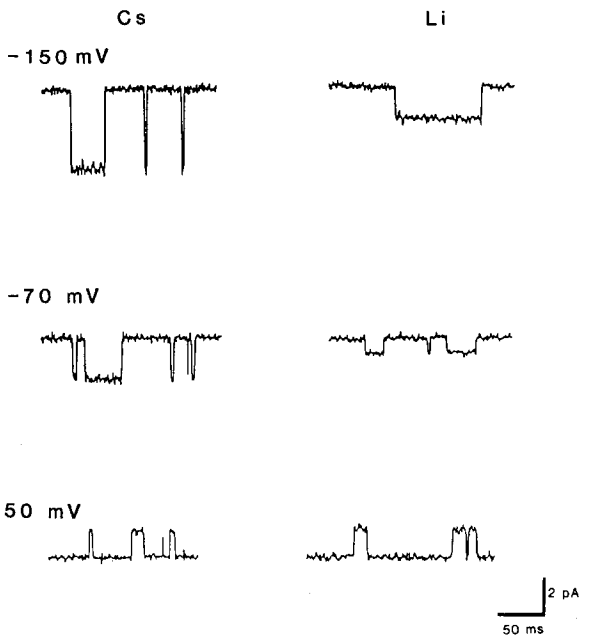

Fig. 8. These records of currents show the effect of the predominant extracellular cation (e.g., Cs or Li, with K being the predominant intracellular cation) on the single-channel current amplitude at various approximate net patch potentials. Temperature 11°C. All records were low-pass filtered at 1 kHz

dependence held, the conductance would be proportional to the permeability and the sequence of conductances would be the same as that of the permeabilities. At potentials more hyperpolarized than about −100 mV, the conductance is virtually constant in each solution. In the case of Li, Na and Cs, the conductance increases gradually from about −100 mV to the null potential. This increase in conductance is most marked for Li. For K, the conductance is virtually constant over this range. For Na, Cs and K at potentials more depolarized than about +30 mV there appears to be a very slight drop in the conductance. Even for K, for which the drop in conductance was clearest, the effect on the *I-V* curve was hardly detectable. For Li, the conduc-

Table 2. Estimates of the null potential (mV) in different cation solutions

Solution	Na	Li	Cs	K
Method of estimation:				
Linear interpolation	−8.0	−20.5	3.7	1.3
Cubic interpolation	−8.1	−18.6	3.3	1.1
Permeability ratios:	0.90	0.56	1.40	1.0

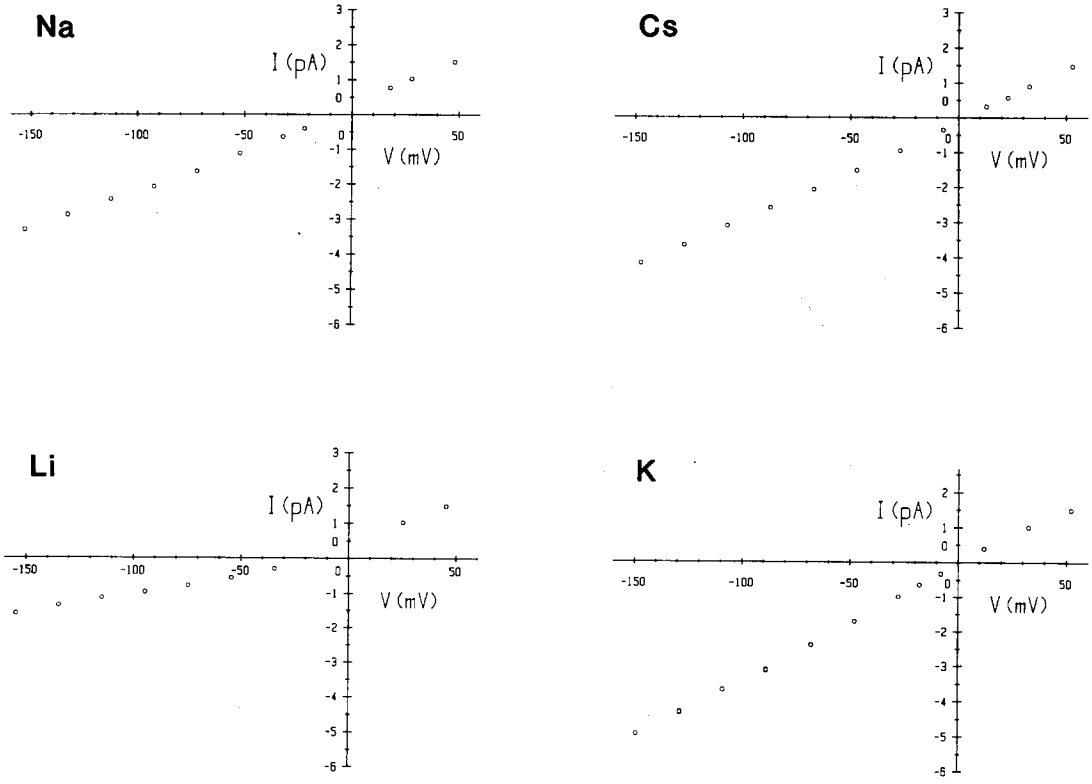

Fig. 9. Experimental current-voltage curve for the four alkali cations tested. Each point represents the grand mean of the mean current from a large number of patches. The error bars represent the SEM. At most potentials the error bars were smaller than the symbols and thus were not shown. The concentration of ACh in the patch-clamp electrode solution was usually between 100 and 300 nM. Temperature 11°C

tance appeared constant at the positive potentials examined. However, a trend similar to that found with the other ions may have been masked for Li since the recording of the currents closer to the null potential was difficult due to the lower conductance of the channels. Finally, a comparison of the conductance at +50 mV with the conductance at −150 mV shows that for Li the conductance has increased by a factor of about 2, for Na there is only a small increase, for Cs the values are similar, and for K there is a decrease in the conductance. The chord conductances at −150 and +50 mV for the various cation solutions are presented in Table 3.

Results of Model Fitting

The two-barrier, single-site, rate-theory model (2B1S model) with uniformly spaced barriers (equidistant from the membrane-solution interface and the centrally placed site; i.e., $d = 0.25$ and 0.75) was not able to provide an adequate fit to the sodium current-voltage curve. However, a good fit to the curve was obtained by altering the locations of the barriers to $d = 0.125$ and 0.875. This gave the same voltage dependence to the rate of entry to the chan-

Table 3. Experimental single-channel chord conductances, $\gamma(V_m)$, at hyperpolarized and depolarized potentials for different ions

Ion	V_m(mV)	$\gamma(V_m)$ (pS)	SEM
Na	−152	23.2	0.4
	+48	26.7	0.9
Li	−152.5	12.1	0.2
	+45.3	23.2	0.5
Cs	−147.1	27.9	0.3
	+52.9	29.4	0.7
K	−148.6	33.1	0.3
	+52.2	29.2	0.5

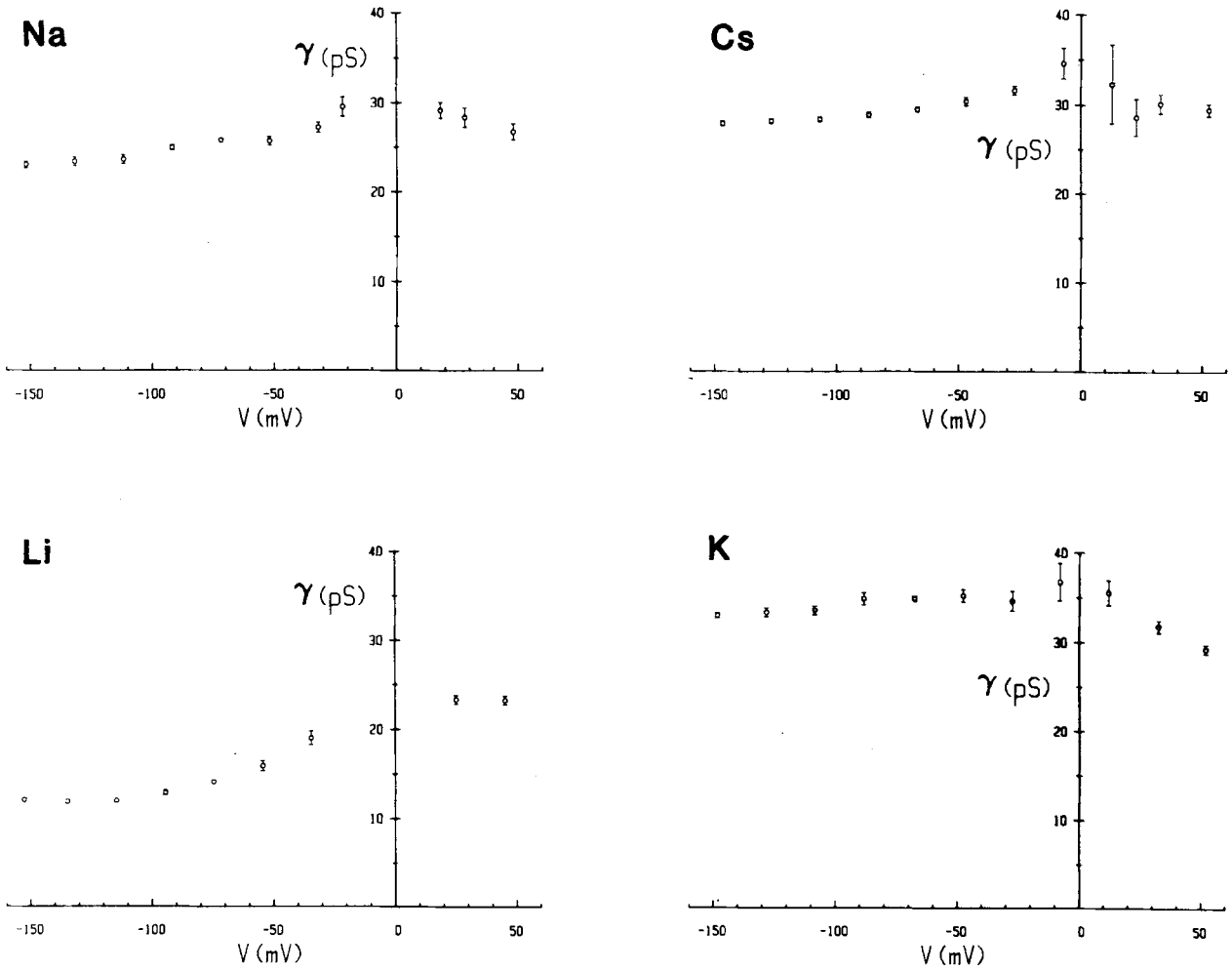

Fig. 10. Experimental chord conductance-voltage relationship for the four alkali cations tested. The chord conductance (γ) was calculated using the null potential estimated by cubic interpolation (*see* Table 2). The error bars represent the SEM. Temperature 11°C

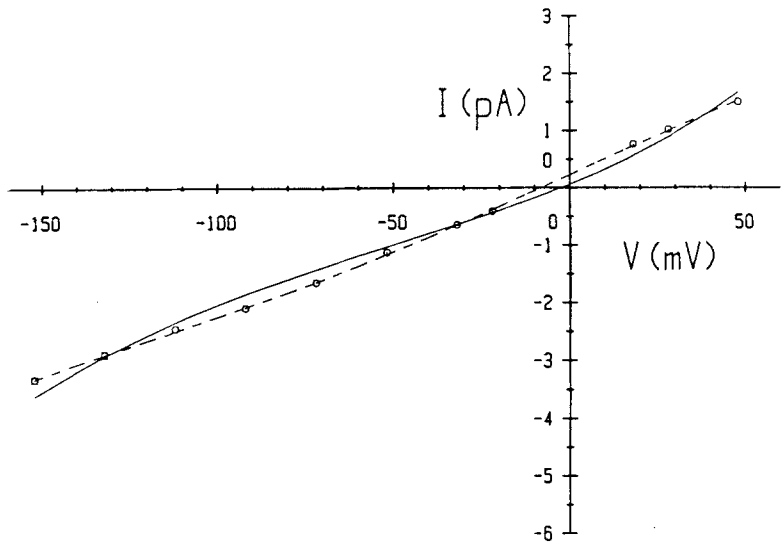

Fig. 11. Predicted *I-V* curves obtained by fitting the 2B1S model to the experimental *I-V* curve for Na. The experimental points are shown as open circles. The continuous line represents the predicted curve of the 2B1S model with the barriers located at $d = 0.25$ and 0.75. The dashed line represents the predicted curve of the 2B1S model with the barriers located at $d = 0.125$ and 0.875

nel as that for the 4B3S model. This model was still symmetrical but had nonuniform barriers. Figure 11 shows the predicted current-voltage curves (*I-V* curves) for both of the 2B1S models and, for comparison, the experimental sodium *I-V* curve. It is clear from a comparison of the two theoretical curves that decreasing the voltage dependence of the rate of entry of the ion to the channel changes the shape of the predicted *I-V* curve from supra- to sublinear. However, despite being able to fit the sodium *I-V* curve, the modified 2B1S model could not adequately fit the lithium *I-V* curve. Even by decreasing the voltage dependence further, it was still not possible to obtain an adequate fit to the lithium *I-V* curve. A fit to the lithium *I-V* curve could probably have been obtained with the 2B1S model by relaxing the condition of symmetry. This approach was not pursued for two main reasons. Firstly, the *I-V* curves for K and Cs were found to be essentially linear over the voltage examined, suggesting a symmetrical energy profile for the major conductive element of the channel. Secondly, as has been pointed out earlier, results recently obtained using excised patches bathed in symmetrical alkali cation solutions all indicate that the energy profile of the major conductive element of the ACh channel is symmetrical (Horn & Patlak, 1980; Redmann et al., 1982; Dwyer & Farley, 1984; Dwyer, 1986; Sanchez et al., 1986). In contrast to the 2B1S model, both the electrodiffusion and the 4B3S rate-theory models gave good fits to the experimental *I-V* curves for Na, Li and Cs. The fitted curves for both models and the experimental data are shown in Fig. 12. Overall, the electrodiffusion model fitted the data more closely. When fitting the 4B3S model, a number of different sets of values for the four free parameters gave an almost identical fit. This was found to be the case for all three ions discussed so far. Closer examination of all the different sets of values found for a particular ion revealed that when each set was rescaled relative to a common parameter, the sets of values all became very similar. Furthermore, the relative permeability, relative binding constant and relative mobility derived from each set of parameter values were found to be all virtually the same. Thus, although it was not possible to estimate uniquely the *absolute* energies involved, it was possible to estimate uniquely and consistently the *relative* energies and ion permeation parameters.

Both the electrodiffusion and the 4B3S model were unable to predict the experimental potassium *I-V* curve using the assumed K concentrations. The fitting of both models was attempted with the internal and external potassium concentrations as free parameters and an acceptable fit was obtained in this way with both models as is shown in Fig. 12. However, for both models the best fit was obtained with the external concentration of potassium greater than the internal concentration. The respective concentrations for the two models were 147 and 125 mM for the 4B3S model, 135 and 113 mM for the electrodiffusion model. The prediction of a higher external concentration is to be expected since the experimental null potential for potassium was positive (*see* Table 2). The fit for the 4B3S model was made significantly better by assuming a symmetrical sodium concentration of 10 mM. A possible interpretation of these results is that the high external potassium concentration caused an alteration of the concentrations of the permeant ions on each side of the patch (*see* Discussion for further details).

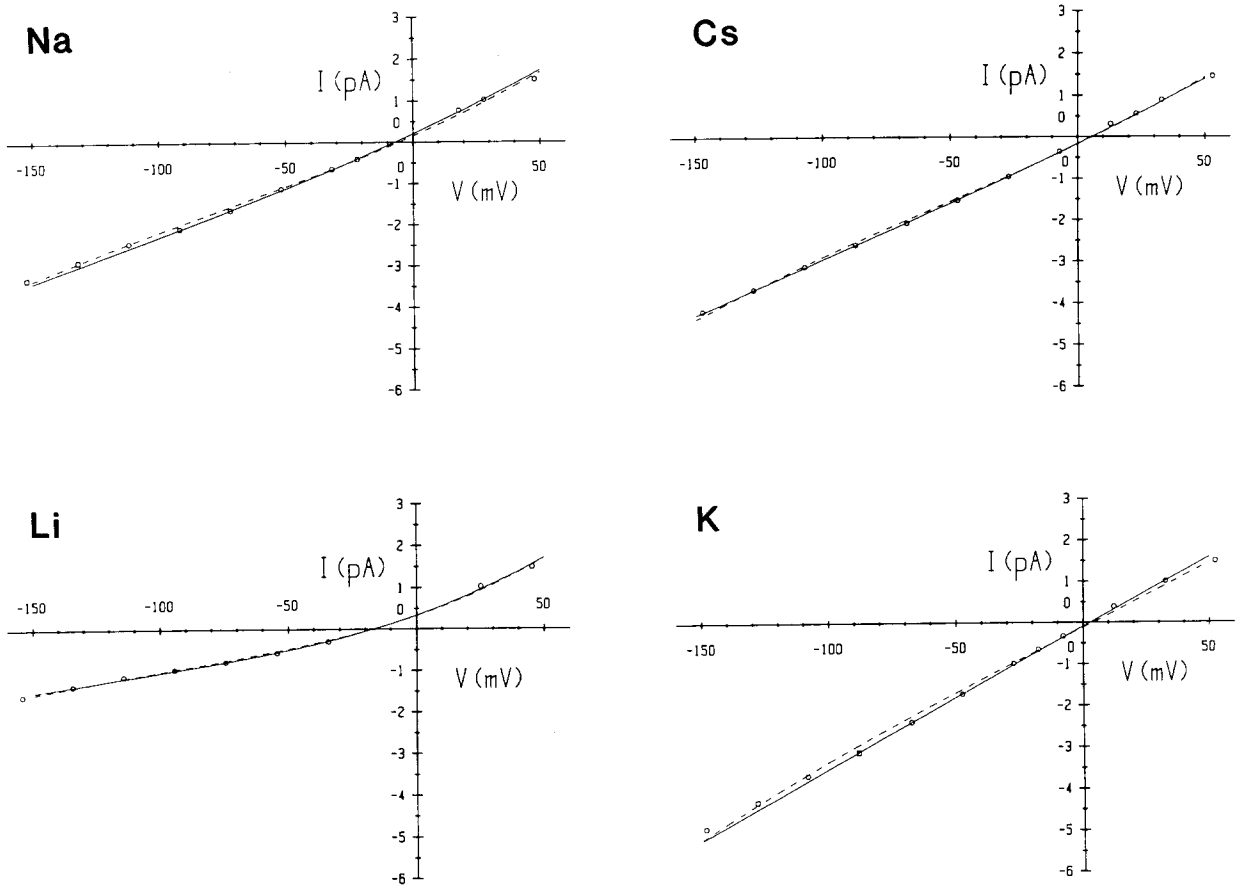

Fig. 12. Predicted *I-V* curves obtained by fitting the electrodiffusion and 4B3S models to the experimental *I-V* curves for the four alkali cations tested. The experimental points are shown as open circles. The continuous lines represent the predicted curves of the electrodiffusion model. The dashed lines represent the predicted curves of the 4B3S model fitted using four free parameters

Table 4 gives the parameters of best fit for the two models tested. Examination of the results for Na shows that the parameters derived from both models agree qualitatively. To clarify the physical meaning of these parameters, an example of the barrier height and well depth found to give an adequate fit to the Na *I-V* curve is shown in Fig. 13. Since the exact shape of the energy profile is unknown, the barrier peaks and well depths are shown connected by straight lines. Similar plots for Li, Cs and K are also shown in Fig. 13. Returning to the case of Na, the relative permeability (P_{Na}/P_K) of approximately 1.0 is due to the almost equal barrier heights (relative to the aqueous solution) for Na and K. Therefore the rates of entry of Na and K into the channel are approximately the same (given the same concentrations). The relative binding constant (K_{Na}/K_K) for sodium was greater than 1.0 due to the greater well depth (relative to the aqueous solution) for Na than for K. The mobility of the ion in the channel is determined by the barrier height relative

Table 4. Model parameters, relative permeability (P_X/P_K), relative binding constant (K_X/K_K), and relative mobility (u_X/u_K)[a]

	Model	
	Rate theory	Electrodiffusion
i) sodium		
P_{Na}/P_K	1.0	0.94
K_{Na}/K_K	2.1	1.6
u_{Na}/u_K	0.49	0.60
ii) lithium		
P_{Li}/P_K	0.59	0.59
K_{Li}/K_K	3.6	3.3
u_{Li}/u_K	0.17	0.18
iii) caesium		
P_{Cs}/P_K	1.6	1.5
K_{Cs}/K_K	2.6	2.06
u_{Cs}/u_K	0.61	0.75

[a] u_X/u_K, the mobility ratio, for the electrodiffusion model is exactly equivalent to k_X/k_K, the transition rate constant ratio, for the rate-theory models.

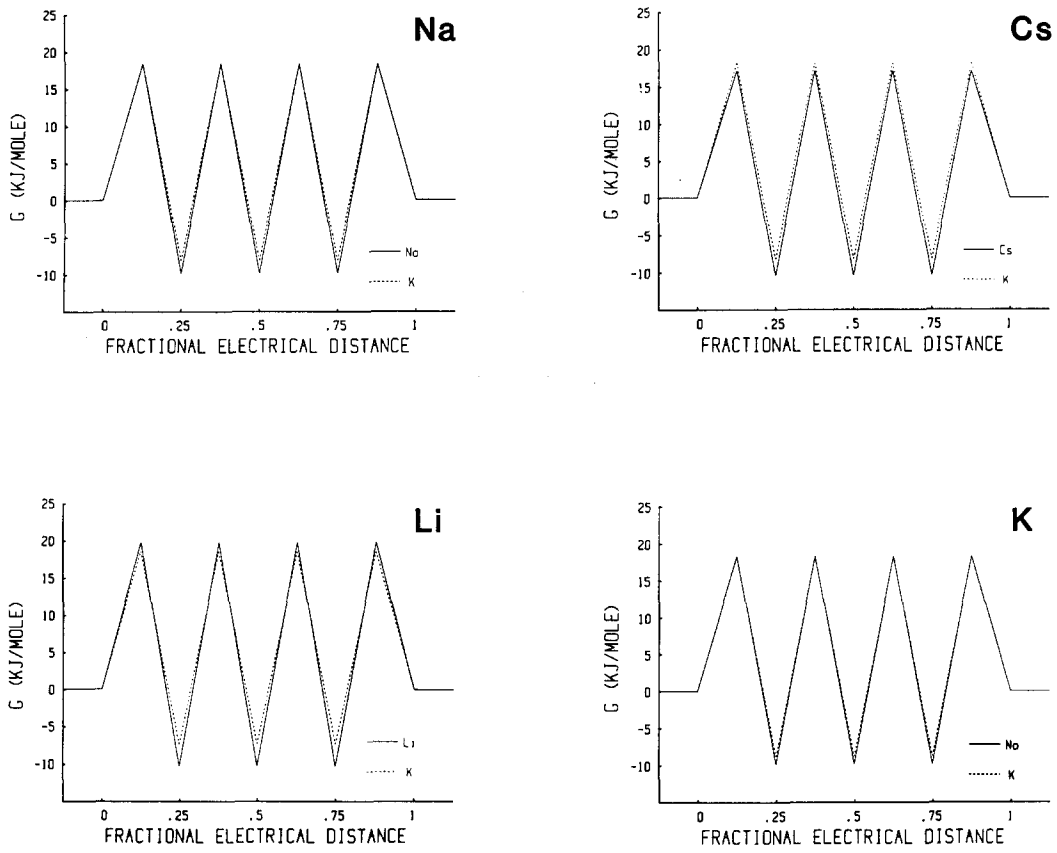

Fig. 13. Examples of the barrier heights and well depths obtained for the 4B3S model for the four alkali cations tested. G represents the voltage-independent component of the Gibb's free energy along the channel, with peaks and wells connected with straight lines for illustrative purposes. Positions 0 and 1 represent the external and internal solution-channel interfaces, respectively. The corresponding values of the relative parameters P_{Na}/P_K, K_{Na}/K_K and u_{Na}/u_K are given in Table 4

to the bottom of the well. This barrier height is greater for Na, hence the relative mobility (u_{Na}/u_K) is less than 1.0.

Examination of Table 4 again (as in the case of Na) shows a good qualitative agreement between the permeation parameters for Li obtained from the 4B3S model and the electrodiffusion model. The barrier height and well depth (relative to the aqueous solution) was greater for Li than K. Correspondingly the relative permeability (P_{Li}/P_K) and mobility (u_{Li}/u_K) were less than 1.0 and the relative binding constant (K_{Li}/K_K) greater than 1.0.

For Cs, the barrier height (relative to the aqueous solution) was less than for K (*see* Fig. 13) so that the relative permeability (P_{Cs}/P_K) was greater than 1.0. But the well depth (relative to the aqueous solution) for Cs was greater than for K, hence the relative binding constant for Cs (K_{Cs}/K_K) is greater than 1.0. The increased well depth for Cs more than offsets its low barrier height so the relative mobility of Cs (u_{Cs}/u_K) is less than 1.0. For Cs there was good qualitative agreement between the permeation parameters obtained from the 4B3S and electrodiffusion models.

Figure 13 shows the barrier heights and well depths found to give the best fit of the 4B3S model to the potassium *I-V* curve. As for Na, the well depth (relative to the aqueous solution) for K was less than that for Na yielding a relative binding constant for Na of 1.59. The barrier heights for Na and K were almost the same giving a relative permeability for Na of 0.96 and a relative mobility for Na of 0.60. Comparing these results with those obtained for Na (*see* Table 4), it appears that the relative binding constant for Na is decreased while the relative mobility of Na is increased in the K solution. Interpretation of these differences is complicated by the fact that the ion concentrations had to be altered to obtain an adequate fit.

As indicated in Table 4, the chord conductances at −150 mV in the respective cation solutions (*see* Table 3) are in the same sequence as the mobilities of the various cations examined. This is to be expected since at −150 mV most of the current is carried by the predominant extracellular cation.

The predicted null potentials, obtained by numerically solving the current equation for each model using the Newton-Raphson technique, are

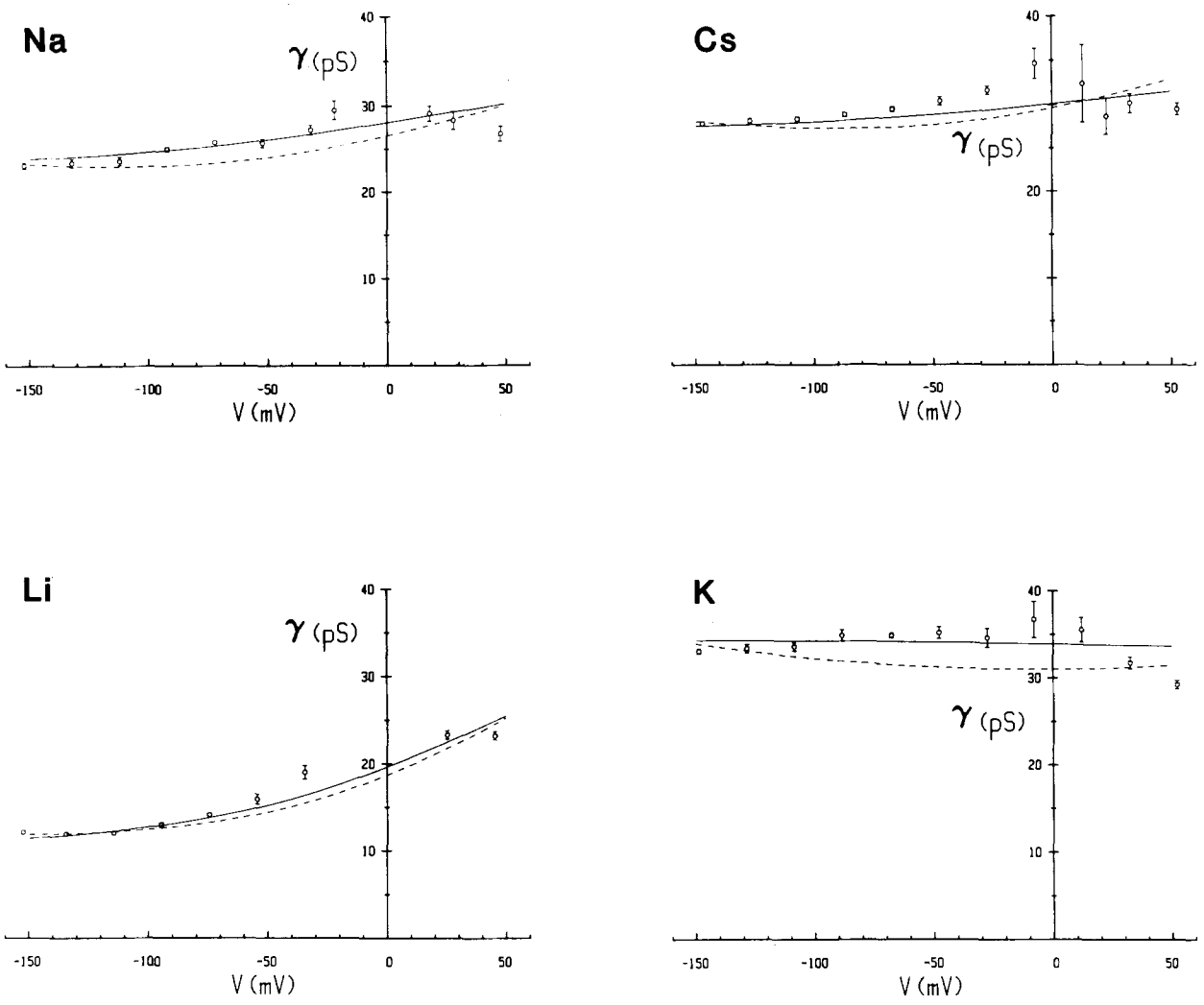

Fig. 14. Chord conductance-voltage curves predicted by the models fitted to the experimental *I-V* curves for the four alkali cations tested. The "experimental" γ-V curve is given by the open circles with the error bars representing the SEM. The continuous lines represent the predictions of the electrodiffusion model while the dashed lines those of the 4B3S model rate-theory model

given in Table 5. The predicted single-channel chord conductance-voltage (γ-V) curves for both models were generated using these null potentials.

The predicted γ-V curves for the various cations are shown in Fig. 14. In each of these Figures, the experimental γ-V curve is also shown for comparison. The discrepancy between the predicted and experimental γ-V curves depends on two factors; firstly, how accurately the model predicted the *I-V* curve and secondly, how closely the model behaved mathematically to the interpolating cubic curve used to estimate empirically the null potential. The electrodiffusion model gave a slightly better fit to the *I-V* curves (*see* Fig. 12) than the 4B3S model. Also the prediction of the null potentials by the electrodiffusion model were closer (except in the case of lithium) to those measured experimentally (*cf.* Tables 5 and 2). These considerations would explain some of the differences between the predicted and experimental curves. It could also explain at least some of the difference between the two predicted curves. However, at potentials more positive than about +30 mV, both models predicted the opposite trend to that seen in the experimental curve. This suggested that another process, besides

Table 5. The null potential (mV) estimated by the electrodiffusion and the 4B3S rate-theory models

Models	Solutions			
	Na	Li	Cs	K
Rate theory	−5.5	−17.3	+6.0	+3.7
Electrodiffusion	−7.1	−17.0	+5.3	+2.5

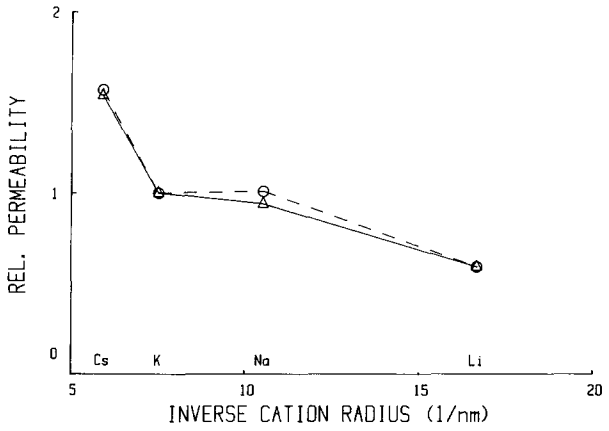

Fig. 15. A plot of the relative permeabilities determined from the models fitted to the experimental *I-V* curves, versus the inverse bare cation radius. The relative permeabilities determined from the electrodiffusion model are given by the triangles connected by a continuous line and those from the 4B3S rate-theory model by circles connected by a dashed line. The lines are of no theoretical significance and simply connect each point for each model

those embodied in the models, was also controlling the conductance at positive potentials. A process that made the entry of ions into the channel rate-limiting, would be consistent with the finding that the decrease in conductance with increasing positive potentials was greatest for K and least for Li.

Examination of the predicted γ-*V* curves for the various cations shows that the voltage dependence of the conductance is different for each cation. Comparing Li, Na, and Cs the increase in the conductance as the potential is depolarized becomes less while for K the conductance is virtually constant. This is also shown in the experimental γ-*V* curves at potentials more negative than the null potential.

A plot of the relative permeability or the relative binding constant against the inverse of the bare cation radius can reveal whether the interaction of the cation with the channel at the location of the barrier or well, respectively, can be explained to a large extent by a simple coulombic model (for a review, *see* Eisenman & Horn, 1983).

Figure 15 shows a plot of the relative permeability versus the inverse of the bare cation radius. The relative permeabilities given by the electrodiffusion model clearly display a "proportional" sequence; that is, the interaction of the ion with the channel at the location of the barriers is probably governed mainly by the relative hydration energy of the cations. As the relative hydration energy is increased, then the rate of entry of the ion to the channel is decreased.

Figure 16 shows a plot of the relative binding constant versus the inverse bare cation radius. This displays a "polarizability" sequence for the results from both the electrodiffusional model and the 4B3S model fitted using four free parameters. Hence a simple coulombic model cannot account for the interaction between the cation and the channel at the well locations.

Discussion

Effects of Alkali Cations

The electrodiffusion model of Barry et al. (1979) and symmetrical rate-theory models with many uniform barriers predict a linear current-voltage curve in symmetrical solutions. The 4B3S model examined predicts an essentially linear *I-V* curve for symmetrical solutions. In contrast, the 2B1S model predicts a symmetrical supralinear curve under the same conditions. In this study it was not possible to record with symmetrical solutions. Recording from excised patches was attempted on several occasions but gave inconsistent results. The reasons were not clear, but may have been due to the damaging effects of Ca^{2+}, in the bath solution, on the cytoplasmic face of the excised patch. Others have also had similar difficulties in recording from excised patches derived from enzyme-treated adult amphibian muscle (O.P. Hamill, *personal communication*). The results presented for K show that in approximately symmetrical solutions the current-voltage curve is essentially linear. However, the *G-V* curve for potassium did show a slight decrease in conductance at potentials more positive than about +30 mV. Further evidence for the symmetry of the channel is given by the results for caesium. Caesium in many respects resembles potassium in terms of the properties known to affect permeation (Hille, 1975*b*; Mullins, 1975; Barry & Gage, 1984). The current-voltage curve for Cs^+ was found to be approximately linear, as expected for a symmetrical channel with at least three sites.

Recordings from excised patches in symmetrical solutions have shown that the current-voltage curve is linear for Na^+ (Horn & Patlak, 1980; Sanchez et al., 1986, rat myotubes), Cs^+ (Dwyer & Farley, 1984; Dwyer, 1986, chick myotubes), and Li^+ (Redmann et al., 1982, cultured BC3H1 cells) but has a slight inward rectification for K^+ (G.A. Redmann, *personal communication*; Sine & Steinbach, 1984*a,b*, both BC3H1 cells). Results for acetylcholine channels reconstituted into planar lipid bilayers have also shown the current-voltage curve to be

linear in symmetrical solutions (Labarca et al., 1984).

The slight inward rectification for K^+ reported by others (G.A. Redmann, *personal communication*; Sine & Steinbach, 1984*a,b*) was not clearly seen in the current-voltage curve obtained for potassium in the present study. The current-voltage curve obtained by Sine and Steinbach (1984*a,b*) shows that the rectification only begins to become prominent at potentials greater than about +50 mV, outside the range of the present study. There is no evidence for rectification at the same potentials for symmetrical Na^+ solutions (Horn & Patlak, 1980) or symmetrical Cs^+ solutions (Dwyer & Farley, 1984). G.A. Redmann (*personal communication*) found, for cell-attached patches with Na^+ in the electrode, that there was rectification at potentials greater than about +100 mV, but that there was no rectification evident for symmetrical solutions of either Na^+ or Li^+. It would appear, therefore, that rectification was observed in every case when potassium was carrying most or all of the outward current. This rectification would be consistent with a diffusion-limited entrance for ions to the channel from the intracellular solution. Andersen (1983) has speculated that diffusion-limited access is not prominent for biological channels because many have antechambers acting as funnels for ions. In contrast, the gramicidin channel does show these effects since it lacks these structures. On this basis, the above hypothesis predicts that there should be no antechamber at the intracellular entrance to the channel, as indeed proposed from other evidence (Horn & Brodwick, 1980; Horn & Stevens, 1980). In summary, the voltage-dependent conductance found for Na^+, Li^+ and Cs^+ over the potential range examined is a consequence of the asymmetrical solutions bathing the membrane.

The voltage sensitivity of conductance for Na found in the present study is significantly lower than that reported previously for extrajunctional channels from the same preparation (Gage & Hamill, 1980). Gage and Hamill found the ratio of the chord conductances in NTR at +30 and −90 mV was approximately 1.9 for extrasynaptic channels and 1.2 for synaptic channels. The value found here for extrajunctional channels was approximately 1.2, the same as the value they obtained for synaptic channels. This is a further example of the inconsistent values of conductance obtained between patch clamping and noise analysis (*see*, for example, Hamill, 1983; Gardener et al., 1984).

The permeability sequence for the alkali cations found in this study is in the same order as their mobilities in aqueous solution, i.e. Li < Na < K < Cs. This agrees with previous findings for junctional

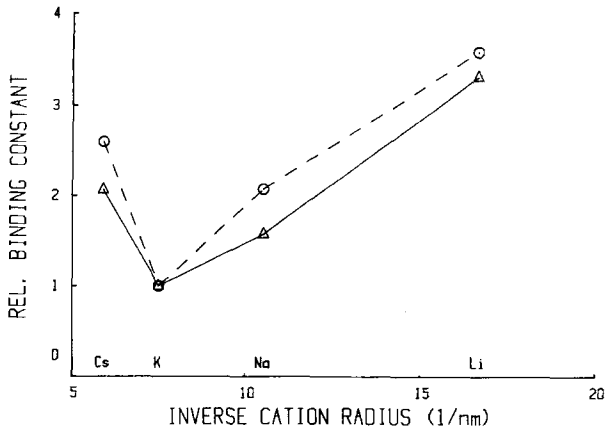

Fig. 16. A plot of the relative binding constant determined from the models fitted to the experimental *I-V* curves, versus the inverse bare cation radius. The relative binding constants determined from the electrodiffusion model are given by the triangles connected by a continuous line and those from the 4B3S rate-theory model by circles connected by a dashed line. The lines have no theoretical significance and simply connect each point for each model

channels found in amphibian muscle (Gage & Van Helden, 1979; Adams et al., 1980; 1981; Lewis & Stevens, 1983). The plot of the relative permeability versus the inverse of the bare cation radius shows a "proportional" selectivity sequence (Eisenman & Horn, 1983). The permeability sequence gives information about the relative interactions of the ions with the part of the channel modelled as an energy peak. The results show the interaction to be approximately inversely proportional to the hydration energy of the ion. In terms of the rate-theory model, this has implications concerning the entrance or association of the ion with the channel. The lower the hydration energy of the ion the more easily it enters the channel. This could be interpreted in several ways. It may indicate partial or complete dehydration of the ion at the time of entry to the channel. Alternatively, it may indicate a diffusion-controlled rate constant for entrance to the channel (Andersen, 1983).

The conductance sequence was Li < Na < Cs < K and was different from the permeability sequence. The conductance sequence is again in agreement with previous findings for junctional channels in amphibian muscle (Gage & Van Helden, 1979; Adams et al., 1981) and for ACh channels found in rat myotubes (Hamill & Sakmann, 1981). The difference in the two sequences shows that the independence principle is violated. For systems obeying independence the conductance ratio sequence should be the same as the permeability ratio sequence. This condition can hold in symmetrical,

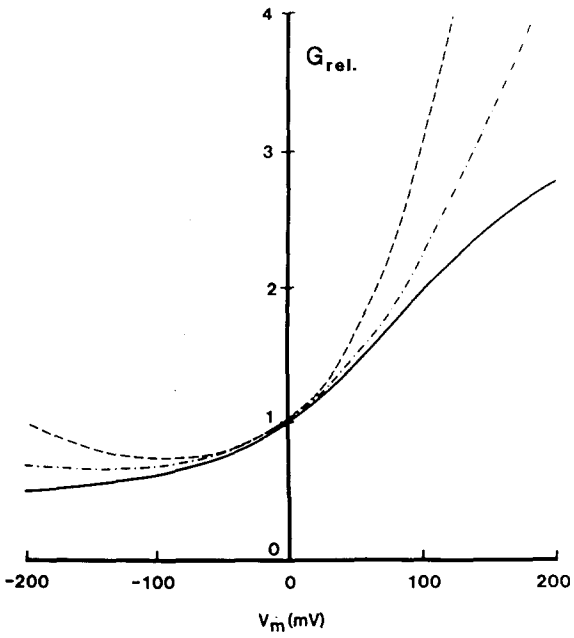

Fig. 17. The relative conductance (G_{rel}) as a function of the net patch potential for symmetrical rate-theory models with uniform barriers (2B1S model, dashed line; 4B3S model, dashed-dotted line) and the electrodiffusion model (solid line). The curves were generated for the biionic solution situation ($A^+X^-:B^+X^-$) assuming equal concentrations for the extracellular (B) and intracellular (A) cations together with the presence of impermeant anions (X^-). Values of $K_A/K_B = 10$ and k_A/k_B (equivalent to u_A/u_B) $= 0.1$ (so that $P_A/P_B = 1$) were assumed for each curve. Redrawn and modified after Barry and Gage (1984)

one-ion channels disobeying independence (such as that examined here) but only in the low concentration limit where the probability that the channel is occupied is very low (Coronado et al., 1980; Eisenman & Horn, 1983). The violation of independence for ion movement through the ACh channel of amphibian muscle has been noted previously in a number of studies on amphibian junctional channels (Lewis, 1979; Lewis & Stevens, 1979; Adams et al., 1981; Takeda et al., 1982*a,b*). Lewis (1979) found that surface charge effects alone were unable to account totally for the violation of the independence of ion movement. Lewis and Stevens (1979) were able to fit the data by adding, in addition to the surface charge effects, competition for an intrachannel site. They proposed a two-barrier, single-site rate-theory model with surface charge effects.

In the model examined in this study, it was assumed that the nonindependent movement of ions through the ACh channel could be accounted for completely by competition for intrachannel sites. As for the number of sites in the channel, the models examined in this study spanned the entire spectrum. For symmetrical channels with uniform barriers and asymmetrical solutions, the effect of increasing the number of sites on the *G-V* curve is shown in Fig. 17. The Figure shows that the most sensitive portions of the voltage range for deciding between models with different numbers of sites are at potentials more hyperpolarized than −100 mV and potentials more depolarized than +50 mV. In particular, the one-site, two-barrier model predicts a supralinear *I-V* curve in the range from −100 to −150 mV. A supralinear *I-V* curve was not found for any of the cations examined in this study. This suggests that the channel has more than one site if a symmetrical model with uniform barriers is assumed. Dwyer and Farley (1984), studying the ACh channel in chick myotubes, have also suggested a symmetrical rate-theory model with more than one site. Recently, Dwyer (1986), studying the ACh channel in chick myotubes, has used a symmetrical 3B2S model to predict the *I-V* curve he obtained for caesium.

The relative binding constants formed a "polarizability" selectivity sequence (Eisenman & Horn, 1983). In terms of the models discussed, the relative binding constant sequence yields information about the relative interactions of the different ions with the intrachannel sites. A polarizability sequence indicates that the attraction between an ion and a site is not just coulombic but requires higher-order terms due to induced dipole interactions. The attraction between the site and cation is strongest for lithium since it has the highest polarizing power.

With the assumed bulk concentrations for sodium and potassium, the Generalized Null Potential Equation and hence both the electrodiffusion and rate-theory models were all unable to adequately fit the potassium *I-V* curve. The bulk concentrations of sodium and potassium contained in the electrode solution were checked independently using a flame spectrophotometer and were found to be the same as those assumed. The null potential for potassium was found to be about +2 mV. This was consistent with both models and indicated that the external K concentration was greater than the internal K concentration. This would point to the bulk intracellular K concentration being lower than the assumed value of 140 mM. Lewis (1979) directly measured the intracellular potassium activity using an ion-sensitive electrode. She found a value of 80 mmol liter^{-1} which was significantly lower than that reported previously by Lev and Armstrong (1975). Lewis speculated the difference may have been a consequence of the microdissection she carried out prior to an experiment. Despite the enzyme treatment used in the present study, the range of the

resting membrane potentials (−70 to −90 mV) of the muscle fibers argues against a significant loss of intracellular potassium. An intracellular potassium concentration of approximately 110 mM could account for the null potential of ≈2 mV found in this study.

Another possibility was that the potassium concentrations adjacent to the membrane were different from those in the bulk solutions. Ayer et al. (1983) found that using isotonic K saline in the patch electrode gave values for the resistance of the membrane patch that were significantly lower than those found using Na saline. Auerbach and Sachs (1984) have suggested that the low membrane patch resistance may have been caused by anomalous rectifier potassium channels that were continuously open in the potassium saline solution. On several occasions in the present study, the amplitude of the current was rechecked after recording for 10 to 15 min using the potassium solution. In each case the amplitude of the current was the same as that at the commencement of recording. Hence, if local concentration changes were occurring adjacent to the membrane patch, it would appear they were established within about a minute of the formation of a gigaohm seal and then remained constant for the recording time. As mentioned previously, the findings of Maruyama and Petersen (1982) and Siegelbaum et al. (1982) suggest a relatively free exchange of material occurs between the general cytoplasm and the cytoplasm adjacent to the membrane patch. This would tend to argue against local concentration changes occurring in the cytoplasm adjacent to the membrane patch. Ayer et al. (1983) also found that the apparent seal resistance was voltage dependent when the patch-clamp electrode contained isotonic K saline. In the present study this should have only produced a negligible error in the voltage across the patch because of the very low input resistance of the cells used.

In summary, the results presented in this paper have shown that the extrajunctional ACh channel in denervated toad muscle has the following characteristics in relation to the permeation of the alkali cations examined:

1. Over the voltage range examined, the channel behaves essentially symmetrically.

2. Independence is violated for the movement of ions through the channel.

3. The current-voltage curve obtained in the various cation solutions can be well fitted by symmetrical channel models based on either electrodiffusion or rate theory.

4. The channel probably has more than one site where interactions with permeating ions take place.

5. The relative permeabilities for the alkali cations examined form a "proportional" selectivity sequence, i.e., $P_{Cs} > P_K > P_{Na} > P_{Li}$.

6. The relative binding constants form a high-field strength "polarizability" selectivity sequence, i.e., $K_{Li} > K_{Cs} > K_{Na} > K_K$.

7. There is a reciprocal relationship between equilibrium constant and mobility so that the more tightly bound ion has the lower mobility in the channel.

We would like to acknowledge the support of the Australian Research Grants Scheme during the course of the project.

References

Adams, D.J., Dwyer, T.M., Hille, B. 1980. The permeability of end-plate channels to monovalent and divalent metal cations. *J. Gen. Physiol.* **75**:493–510

Adams, D.J., Nonner, W., Dwyer, T.M., Hille, B. 1981. Block of end-plate channels by permeant cations in frog skeletal muscles. *J. Gen. Physiol.* **78**:593–615

Andersen, O.S. 1983. Ion movement through Gramicidin A channels. Studies on the diffusion-controlled association step. *Biophys. J.* **41**:147–165

Anderson, C.R., Stevens, C.F. 1973. Voltage-clamp analysis of acetylcholine produced end-plate current fluctuations at the neuromuscular junction. *J. Physiol. (London)* **235**:655–691

Auerbach, A., Sachs, F. 1984. Patch clamp studies of single ionic channels. *Annu. Rev. Biophys. Bioeng.* **13**:269–302

Ayer, R.K., Jr., De Haan, R.L., Fischmeister, R. 1983. Measurement of membrane patch and seal resistance with two patch electrodes in chick embryo cardiac cells. *J. Physiol. (London)* **345**:29P

Barford, N.C. 1967. Experimental Measurements: Precision, Error and Truth. Addison-Wesley, London

Barry, P.H., Diamond, J.M. 1970. Junction potentials, electrode standard potentials, and other problems in interpreting electrical properties of membranes. *J. Membrane Biol.* **3**:93–122

Barry, P.H., Gage, P.W. 1984. Ionic selectivity of channels at the end-plate. *In:* Ion Channels: Molecular and Physiological Aspects. W.D. Stein, editor. Ch. 1, pp. 1–51. Academic, New York

Barry, P.H., Gage, P.W., Van Helden, D.F. 1979. Cation permeation at the amphibian motor end-plate. *J. Membrane Biol.* **45**:245–276

Camardo, J.S., Siegelbaum, S.A. 1983. Single channel analysis in *Aplysia* neurones. A specific K^+ channel is modulated by serotonin and cyclic AMP. *In:* Single Channel Recording. B. Sakmann and E. Neher, editors. Ch. 21, pp. 409–423. Plenum, New York

Corey, D.P., Stevens, C.F. 1983. Science and technology of patch-recording electrodes. *In:* Single-Channel Recording. B. Sakmann and E. Neher, editors. Ch. 3, pp. 53–68. Plenum, New York

Coronado, R., Rosenberg, R.L., Miller, C. 1980. Ionic selectivity, saturation and block in a K^+-selective channel from sarcoplasmic reticulum. *J. Gen. Physiol.* **76**:425–446

Dulhunty, A.F., Gage, P.W. 1973. Electrical properties of toad sartorius muscle fibers in summer and winter. *J. Physiol. (London)* **230:**619–641

Dwyer, T.M. 1986. Guanidine block of single channel currents activated by acetylcholine. *J. Gen. Physiol.* **88:**635–650

Dwyer, T.M., Adams, D.J., Hille, B. 1980. The permeability of end-plate channels to organic cations in frog muscle. *J. Gen. Physiol.* **75:**469–492

Dwyer, T.M., Farley, J.M. 1984. Permeability properties of chick myotube acetylcholine-activated channels. *Biophys. J.* **45:**529–539

Eisenman, G., Horn, R. 1983. Ionic selectivity revisited: The role of kinetic and equilibrium processes in ion permeation through channels. *J. Membrane Biol.* **76:**197–225

Eyring, H. 1935. The activated complex in chemical reactions. *J. Chem. Phys.* **3:**107–115

Fenwick, E.M., Marty, A., Neher, E. 1982. A patch clamp study of bovine chromaffin cells and of their sensitivity to acetylcholine. *J. Physiol. (London)* **331:**577–597

Gage, P.W., Hamill, O.P. 1980. Lifetime and conductance of acetylcholine-activated channels in normal and denervated toad sartorius muscle. *J. Physiol. (London)* **298:**525–538

Gage, P.W., Van Helden, D.F. 1979. Effects of permeant monovalent cations on end-plate channels. *J. Physiol. (London)* **288:**509–528

Gagne, S., Plamondon, R. 1983. Tip potential of open tip glass microelectrodes: Theoretical and experimental studies. *Can. J. Physiol. Pharmacol.* **61:**857–869

Gardener, P., Ogden, D.C., Colquhoun, D. 1984. Conductances of single ion channels opened by nicotinic agonists are indistinguishable. *Nature (London)* **309:**160–162

Glasstone, S., Laidler, K.J., Eyring, H. 1941. The Theory of Rate Processes. McGraw-Hill, New York

Goldman, D. 1943. Potential, impedance and rectification in membranes. *J. Gen. Physiol.* **27:**37–60

Hamill, O.P. 1983. Membrane ion channels. *In:* Topics in Molecular Pharmacology. A.S.V. Burgen and G.C.K. Roberts, editors. pp. 181–205. Elsevier Science Publishers, Amsterdam

Hamill, O.P., Marty, A., Neher, E., Sakmann, B., Sigworth, F.J. 1981. Improved patch-clamp techniques for high resolution current recording from cells and cell free membrane patches. *Pfluegers Arch.* **391:**85–100

Hamill, O.P., Sakmann, B. 1981. Multiple conductance states of single acetylcholine receptor channels in embryonic muscle cells. *Nature (London)* **294:**462–464

Hille, B. 1975*a*. Ionic selectivity, saturation and block in sodium channels. A four-barrier model. *J. Gen. Physiol.* **66:**535–560

Hille, B. 1975*b*. Ionic selectivity of Na and K channels of nerve membranes. *In:* Membranes—A Series of Advances. G. Eisenman, editor. Vol. 3, Ch. 4, pp. 255–323. Marcel Dekker, New York

Hodgkin, A.L., Katz, B. 1949. The effects of sodium ions on the electrical activity of the giant axon of the squid. *J. Physiol. (London)* **108:**37–77

Horn, R., Brodwick, M.S. 1980. Acetylcholine-induced current in perfused rat myoballs. *J. Gen. Physiol.* **75:**297–321

Horn, R., Patlak, J. 1980. Single channel currents from excised patches of muscle membranes. *Proc. Natl. Acad. Sci. USA* **77:**6930–6934

Horn, R., Stevens, C.F. 1980. Relation between structure and function of ion channels. *Com. Mol. Cell Biophys.* **1:**57–68

Labarca, P., Lindstrom, J., Montal, M. 1984. Acetylcholine receptors in planar lipid bilayers. *J. Gen. Physiol.* **83:**473–496

Lev, A.A., Armstrong, W. McD. 1975. Ion activities in cells. *Curr. Top. Membr. Transp.* **6:**59–123

Lewis, C.A. 1979. Ion concentration dependence of the reversal potential and the single channel conductance of ion channels at the frog neuromuscular junction. *J. Physiol. (London)* **286:**417–445

Lewis, C.A., Stevens, C.F. 1979. Mechanisms of ion permeation through channels in a post-synaptic membrane. *In:* Membrane Transport Processes. C.F. Stevens and R.W. Tsien, editors. pp. 133–151. Raven, New York

Lewis, C.A., Stevens, C.F. 1983. Acetylcholine receptor channel ionic selectivity: Ions experience an aqueous environment. *Proc. Natl. Acad. Sci. USA* **80:**6110–6113

MacInnes, D.A. 1961. The Principles of Electrochemistry. Dover, New York

Maeno, T., Edwards, C., Anraku, M. 1977. Permeability of end-plate membrane activated by acetylcholine to some organic cations. *J. Neurobiol.* **8:**173–184

Maruyama, Y., Petersen, O.H. 1982. Cholecystokinin activation of single channel currents is mediated by internal messenger in pancreatic acinar cells. *Nature (London)* **300:**61–63

Mullins, L.J. 1975. Ion selectivity of carriers and channels. *Biophys. J.* **15:**921–931

Neher, E., Sakmann, B., Steinbach, J.H. 1978. The extracellular patch clamp: A method for resolving currents through individual open channels in biological membranes. *Pfluegers Arch.* **375:**219–230

Purves, R.D. 1981. Microelectrode Methods for Intracellular Recording and Ionophoresis. Academic, London

Rae, J.L., Levis, R.A. 1984. Patch voltage clamp of lens epithelial cells: Theory and practice. *Mol. Physiol.* **6:**115–162

Redmann, G.A., Clark, R.B., Adams, P.R. 1982. Single acetylcholine channel block in elevated sodium and lithium. *Biophys. J.* **37:**324a

Robinson, R.A., Stokes, R.H. 1965. Electrolyte Solutions. (2nd Ed.) Butterworth, London

Sakmann, B., Neher, E. 1983. Geometric parameters of pipettes and membrane patches. *In:* Single-Channel Recording. B. Sakmann and E. Neher, editors. Ch. 2, pp. 37–51. Plenum, New York

Sanchez, J.A., Dani, J.A., Siemen, D., Hille, B. 1986. Slow permeation of organic cations in acetylcholine receptor channels. *J. Gen. Physiol.* **87:**985–1001

Siegelbaum, S.A., Camardo, J.S., Kandel, E.R. 1982. Serotonin and cyclic AMP close single K^+ channels in *Aplysia* sensory neurones. *Nature (London)* **299:**413–417

Sine, S.M., Steinbach, J.H. 1984*a*. Activation of a nicotinic acetylcholine receptor. *Biophys. J.* **45:**175–185

Sine, S.M., Steinbach, J.H. 1984*b*. Agonists block currents through acetylcholine receptor channels. *Biophys. J.* **46:**277–284

Takeda, K., Barry, P.H., Gage, P.W. 1980. Effects of ammonium ions on end-plate channels. *J. Gen. Physiol.* **75:**589–613

Takeda, K., Barry, P.H., Gage, P.W. 1982*a*. Effects of extracellular sodium concentrations on null potential, conductance and open time of end-plate channels. *Proc. R. Soc. London B* **216:**225–251

Takeda, K., Gage, P.W., Barry, P.H. 1982*b*. Effects of divalent cations on toad end-plate channels. *J. Membrane Biol.* **64:**55–66

Takeuchi, A., Takeuchi, N. 1959. Active phase of frog's end-plate potential. *J. Neurophysiol.* **22:**395–411

Takeuchi, A., Takeuchi, N. 1960. On the permeability of end-plate membrane during the action of transmitter. *J. Physiol. (London)* **154:**52–67

Van Helden, D.F., Hamill, O.P., Gage, P.W. 1977. Permeant cations alter end-plate channel characteristics. *Nature (London)* **269:**711–713

Woodbury, J.W. 1971. Eyring rate-theory model of the current-voltage relationships of ion channels in excitable membranes. *In:* Chemical Dynamics: Papers in Honor of Henry Eyring. J.O. Hirschfelder, editor. pp. 601–617. Wiley, New York

Received 5 January 1987; revised 23 February 1987